

Monsoonal intensity dominated the Eocene evolution of paleovegetation and paleoclimate in northern South China Sea

Jinhua Zeng^a, Tao Jiang^{a,*}, Keqiang Wu^b, Desheng Hu^b, Yong Man^b, Licheng Cao^a, Cong Cheng^{a,c}, Zigui Chen^{a,b}, Kun Wang^d, Nan Bai^b, Meiling Feng^a, Ziyi Li^a

^a Hubei Key Laboratory of Marine Geological Resources, China University of Geosciences, Wuhan 430074, China

^b Zhanjiang Branch Company, China National Offshore Oil Corporation, Zhanjiang 524057, China

^c Institute for Advanced Marine Research, China University of Geosciences, Guangzhou 511462, China

^d Guangzhou Marine Geological Survey, China Geological Survey, Guangzhou 511458, China

ARTICLE INFO

Editor: Dr. Howard Falcon-Lang

Keywords:

Paleovegetation
Paleoclimate
East Asian summer monsoon
Northern South China Sea
Weixinan Sag

ABSTRACT

The East Asian climate system experienced profound transformation throughout the Eocene epoch, characterized by spatial differences in paleoclimate evolution. However, continuous records of Eocene climate remain scarce, and the driving mechanisms are poorly understood, particularly in low-latitude regions. The Weixinan Sag in the northern South China Sea documents vegetation dynamics and weathering regimes through its continuous clastic sedimentary sequences. Based on palynological records and geochemical proxies from the Eocene Liushagang Formation in the Weixinan Sag, this study suggests a triphasic climatic evolution in the northern South China Sea. During the early Eocene, the Weixinan Sag was dominated by floodplain deciduous broad-leaved forests and montane coniferous forests under moderate weathering conditions, signaling a subtropical monsoon climate. By the middle Eocene, enhanced rainfall triggered peak humidity with intense chemical weathering, alongside the development of evergreen-deciduous broadleaved forests in lowlands and mixed forests in highlands. During the late Eocene, aridification resulted in fern expansion and diminished weathering, yet residual rainfall rhythms persisted. Paleovegetation landscapes and chemical weathering intensity, marked by seasonal precipitation fluctuations, confirm operational monsoonal circulation since the early Eocene and demonstrate the dominance of monsoonal circulation in the Eocene climate of the northern South China Sea. Weak coastal proto-monsoonal cells initiated in early Eocene low-latitude coastal areas through greenhouse-enhanced land-sea thermal gradients, matured into a continental-scale system during middle Eocene paleogeographic restructuring, and then attenuated in the late Eocene due to the effects of global cooling on thermal gradients overriding that of paleogeographic changes. These findings not only reveal the Eocene climatic evolution and driving mechanisms in low-latitude regions, but also recalibrate the developmental chronology of the Eocene East Asian summer monsoon.

1. Introduction

The Eocene epoch was one of the warmest intervals in the Cenozoic, characterized by climatic conditions fundamentally distinct from the present (Pearson and Palmer, 2000; Zachos et al., 2008; Huber and Caballero, 2011). During the Eocene, the global temperature was approximately 8–13 °C higher than present-day values, primarily driven by elevated atmospheric pCO_2 (Pearson and Palmer, 2000; Beerling and Royer, 2011; Foster et al., 2017; Burke et al., 2018). The latitudinal surface temperature gradient remained remarkably weak, with only a ~

20 °C difference between equatorial and polar regions, significantly lower than modern 38 °C (Zachos et al., 1994; Greenwood and Wing, 1995; Pearson et al., 2007; Zhu et al., 2019). Under this hyperthermal background, multiple short-term extreme thermal events added complexity to global climatic evolution, exerting profound impacts on terrestrial ecosystems and biological evolutionary trajectories (Zachos et al., 2001; Yapp, 2004; Bouchenak-Khelladi et al., 2009; Henry and Vallis, 2022).

In East Asia, the Eocene climatic evolution exhibited pronounced spatial heterogeneity shaped by the interplay of global temperature

* Corresponding author.

E-mail address: taojiang@cug.edu.cn (T. Jiang).

forcing and regional tectonic-climatic feedbacks (Cai and Kong, 2024). In Central China, sedimentary and palynological records reveal a significant climatic shift from early Eocene aridity to mid – late Eocene periodic humidity, marked by a decline in arid components and the replacement of underlying red beds with salt rhythmic layers. This shift is widely interpreted as signaling the incipient establishment of East Asian summer monsoon (EASM) system (Tong et al., 2001; Wang et al., 2013; Xie et al., 2022; Kong et al., 2024; Cai and Kong, 2024). The hypothesis is supported by vegetation patterns in South China, where the mid-late Eocene vegetation assemblages were composed of mixed evergreen and deciduous broad-leaved forests similar to those found in monsoon-zone communities, indicating a warm-humid subtropical climate with distinct seasonal rainfall and temperature (Li, 1998; Spicer et al., 2014; Aleksandrova et al., 2015; Xie et al., 2019). In Southwest China, a notable vegetation shift occurred around 41 Ma, demonstrating a consistent sudden switch from a hot-dry environment to a seasonally wet climate in the, which was evidenced for the expansion of the Asian monsoon, specifically the northward advance of the Indian monsoon (Fang et al., 2021; Wu et al., 2022; Wu et al., 2024). Additionally, in Northeast China, paleoclimatic evolution generally aligned with the trend of temperature records in deep-sea $\delta^{18}\text{O}$, (Quan et al., 2012a; Meng et al., 2018). In contrast, northwestern China experienced aridification during the mid-late Eocene, evidenced by the growth of *Ephedra*-dominated shrub desert and widespread deposition of evaporites and red beds (Miao et al., 2016; Sayem et al., 2018).

This regional climatic differentiation has complicated unified understanding of East Asian Eocene climate evolution while hindering comprehension of its driving mechanisms. The East Asian summer monsoon system is widely considered to have been established during the Eocene, recognized as a major driver of regional paleoclimate (Wang

et al., 2013; Ye et al., 2022; Xie et al., 2022). Its formation may be linked to global atmospheric CO_2 levels and regional tectonic activity (Anagnostou et al., 2016; Liu et al., 2017; Farnsworth et al., 2019; Xie et al., 2022). Key regional tectonic drivers included: (1) the Tibetan Plateau uplift initiated by the early Eocene India-Eurasia collision, with paleoaltimetry data indicating mid-late Eocene elevations exceeding 4500 m in central Tibet (Wang et al., 2014; Ding et al., 2014; Renner, 2016); (2) the dramatic regression of the Paratethys Sea, amplifying land-sea thermal contrasts (Bosboom et al., 2011; Sun and Jiang, 2013; Guo et al., 2022); and (3) orographic growth of the Southeast Mountains beyond 2000 m elevation, which redirected atmospheric circulation (Zhang et al., 2012; Zhang et al., 2022).

However, incomplete sedimentary records constrain overall understanding of Eocene climate evolution, which hinders comprehension of East Asian summer monsoon development, particularly in low-latitude regions. The Weixinan Sag, one of petrolierous basins, is located on the continental shelf of the northern South China Sea. During the Eocene, the Weixinan Sag was situated within the tropical-subtropical climatic transition zone with a paleolatitude of $\sim 20^\circ\text{N}$ and developed continuous clastic sequences (Scotese, 2016). Its proximity to the Pacific moisture source and sensitivity to monsoonal dynamics make it an exceptional archive for investigating the Eocene low-latitude climate conditions and developmental framework about EASM. Through integrated analysis of elemental geochemistry and palynological records from the Eocene Liushagang Formation in the Weixinan Sag, this paper aims to systematically reconstruct the paleovegetation succession and paleoclimatic evolution in the northern South China Sea. It further seeks to elucidate underlying paleoclimatic drivers and the development of the EASM.

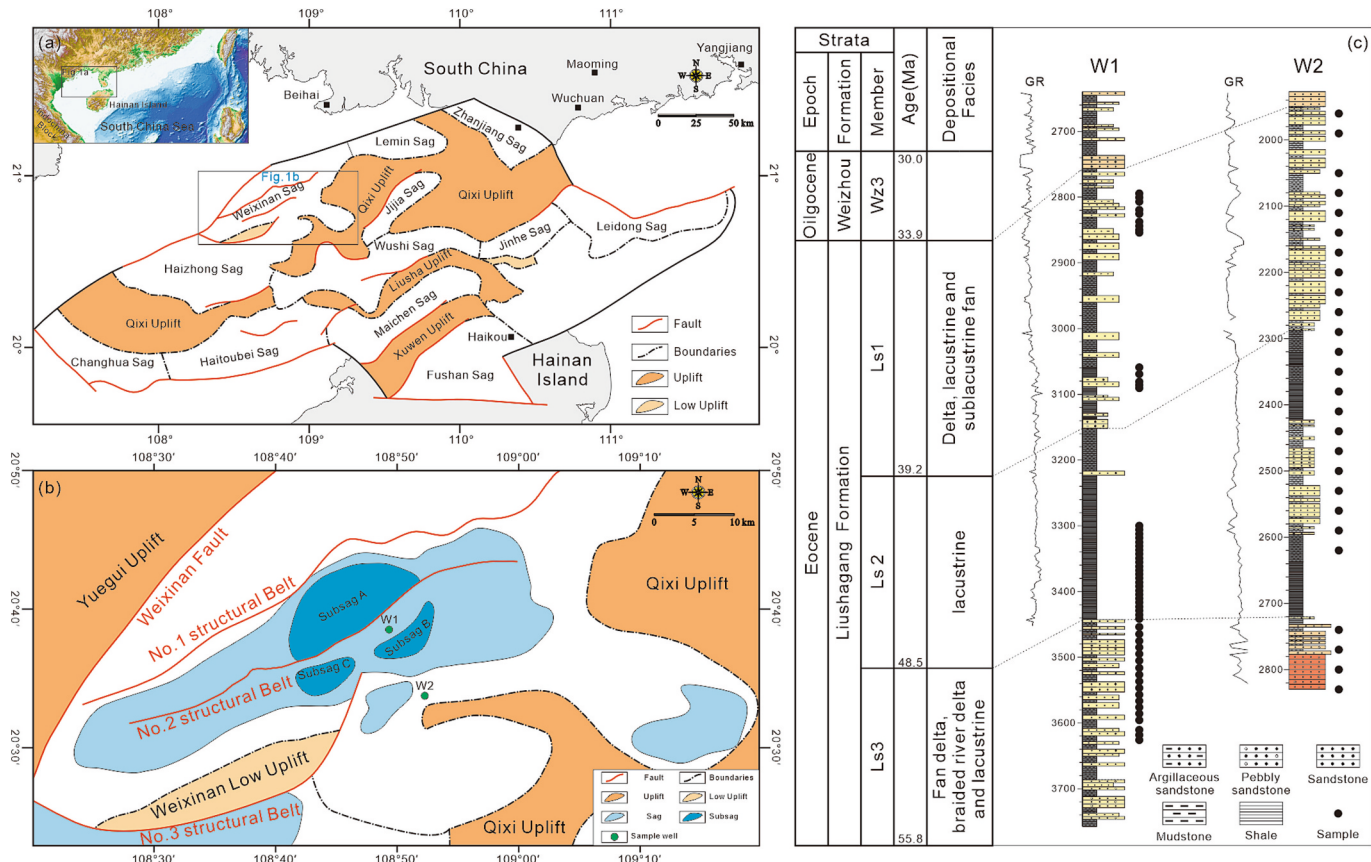


Fig. 1. Tectonic map and profile of the Weixinan Sag, Beibuwan Basin (modified after Zhao et al., 2020). (a) structural divisions of the Beibuwan Basin. (b) structural divisions of the Weixinan Sag and the location of boreholes W1 and W2. (c) stratigraphic division and lithological characteristics of the Liushagang Formation from boreholes W1 and W2.

2. Regional geological setting

The Weixinan Sag, located in the northern Beibuwian Basin, is structurally bounded by the Haizhong Sag to the east and the Lemin Sag to the west (Fig. 1a). During the Eocene, the Weixinan Sag received sufficient sediment supply, accumulating lacustrine clastic sequences of the Liushagang Formation. Based on lithofacies variations, the Liushagang Formation can be stratigraphically subdivided into three members. The lower member (Ls3) was deposited in a shallow lacustrine environment dominated by braided river delta conglomerates and sandstones, exhibiting upward-fining grain size trends. The middle member (Ls2) developed thick, deep lacustrine black mudstones and shales, representing the maximum paleowater depth during the depositional phase. The upper member (Ls1) comprised delta and sublacustrine fan deposits, primarily consisting of fine-grained sandstones interbedded with mudstones (Fig. 1c).

Oxygen isotope dating and astronomical timescale dating indicate that the Liushagang Formation developed approximately between 55.8 and 33.9 Ma. The boundary between Ls1 and Ls2 is approximately 39.2 Ma, and that between Ls2 and Ls3 is about 48.5 Ma (Cao et al., 2016; Wei, 2021). Based on sedimentation rates and astronomical cycle analysis, Ls3 was deposited from 55.8 to 48.5 Ma, with the boundary between its upper and lower sub-members dated at around 51.94 Ma. The lower sub-member lasted about 3.86 Ma, while the upper sub-member persisted for approximately 3.44 Ma. Ls2 developed between 48.5 and 39.2 Ma, with the boundary between its upper and lower sub-members at approximately 46.47 Ma. The lower sub-member extended for about 2.03 Ma, and the upper sub-member lasted around 7.27 Ma. Ls1 was deposited from 39.2 to 33.9 Ma and exhibits relatively consistent sedimentation rates within the unit (Wei et al., 2018; Li et al., 2023) (Fig. 2).

Regarding its sedimentary background, Xie et al. (2012) proposed

that the Liushagang Formation was entirely deposited under subtropical humid climatic conditions. This interpretation is supported by sporopollen assemblages and the Carbon Preference Index (CPI). Li et al. (2019) reported high proportions of evergreen components and low proportions of deciduous components in the middle-late Eocene strata. Ye et al. (2020) further noted that CPI values generally exceed the aridity threshold throughout the Liushagang Formation, with Ls2 showing the highest CPI value (mean = 1.67), followed by Ls1 (mean = 1.48), and Ls3 exhibiting relatively lower value (mean = 1.41). In contrast, Liu et al. (2025) suggested a potential trend toward persistent aridification based on progressively increasing mesophytic taxa and decreasing hygrophytic elements in sporopollen assemblages.

3. Materials and methods

In this study, core samples from the Liushagang Formation were systematically collected from continuously cored exploration boreholes W1 and W2 in the Weixinan Sag, Beibuwian Basin (Fig. 1b). After being cleaned to remove impurities and dust, the samples were transferred to the Zhanjiang Laboratory of China National Offshore Oil Corporation for analytical testing.

3.1. Elemental analysis

A total of 63 samples from borehole W1 were analyzed for major and trace elements. The samples were ground to 200 mesh and subsequently analyzed for major elements using wavelength-dispersive X-ray fluorescence spectrometry (XRF), while trace elements were measured by inductively coupled plasma mass spectrometry (ICP-MS). The analytical procedures followed Chinese national standards GB/T 14506.28–2010 and GB/T 14506.30–2010 (Methods for Chemical Analysis of Silicate

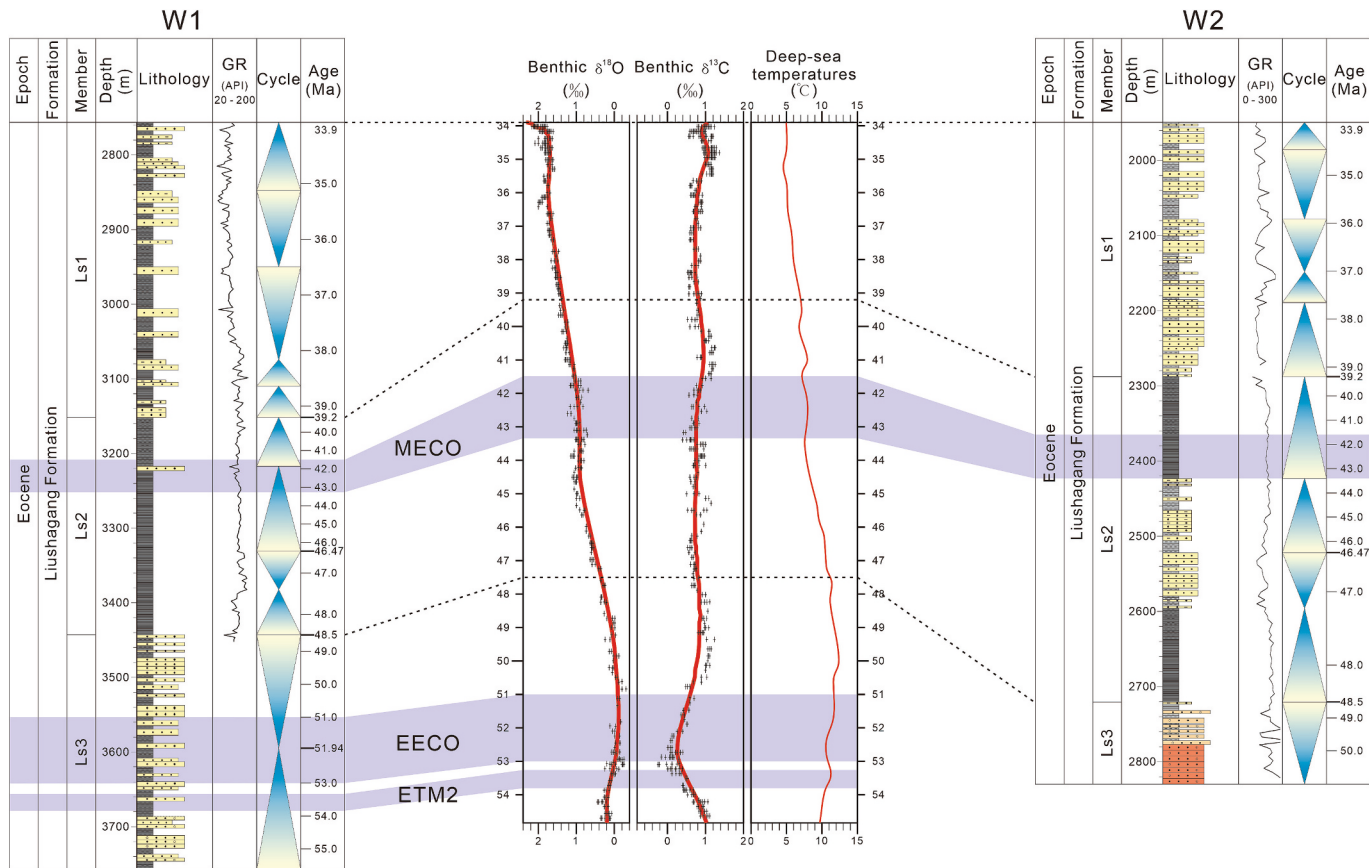


Fig. 2. Comparison of the sedimentary records and ages from boreholes W1 and W2 with the global records of benthic $\delta^{18}\text{O}$, benthic $\delta^{13}\text{C}$, and deep-sea temperature during the Eocene (Zachos et al., 2001; Zachos et al., 2008; Wei et al., 2018; Li et al., 2023).

Rocks). The results are presented in Table S-1. The analytical precision was better than 1 % for major elements, and 5 % for trace elements.

3.2. Palynological analysis

A total of 30 samples were collected from borehole W2 at 30 m intervals for Palynological analysis. The samples were processed following standard procedures. Specifically, 30 g of sieved dried sample was first treated with 10 % HCl and 40 % HF to remove carbonates and silicates. The residue was then sieved with a 6 μm mesh size, and mounted on slides with glycerin gelatin for identification under a microscope. Among the 30 samples, 26 samples contained abundant pollen and spores, while the remaining 4 samples were very poor. All sample processing and identification were conducted at the Zhanjiang Laboratory of China National Offshore Oil Corporation, in strict compliance with the Chinese national oil and gas industry standard SY/T 5915–2000.

4. Results

4.1. Major and trace elements

The analytical results reveal pronounced compositional variations in the major and trace elements of the Liushagang Formation (Table S1).

Compared to the average content of Post-Archean Australian Shale (PAAS) (Taylor and McLennan, 1985), the Liushagang Formation exhibits marginally higher average concentrations of MnO and P₂O₅, alongside lower contents of Al₂O₃, Fe₂O₃, MgO, CaO, Na₂O, K₂O, and TiO₂. Among them, the Ls3 is characterized by elevated Al₂O₃ (avg. 17.46 %), MgO (avg. 1.22 %), and K₂O (avg. 3.33 %), with lower Fe₂O₃ (avg. 5.92 %), CaO (avg. 0.54 %), Na₂O (avg. 0.39 %), MnO (avg. 0.10

%), and P₂O₅ (avg. 0.11 %). The Ls2 shows enrichment in Fe₂O₃ (avg. 6.98 %), CaO (avg. 1.05 %), MnO (avg. 0.18 %), and P₂O₅ (avg. 0.33 %), contrasting with lower Al₂O₃ (avg. 16.36 %), MgO (avg. 1.05 %), Na₂O (avg. 0.39 %), and K₂O (avg. 2.39 %). The Ls1 is distinguished by higher Al₂O₃ (avg. 18.61 %), MgO (avg. 1.95 %), CaO (avg. 0.86 %), Na₂O (avg. 0.53 %), and K₂O (avg. 3.50 %), while displaying reduced Fe₂O₃ (avg. 5.71 %), MnO (avg. 0.05 %), and P₂O₅ (avg. 0.13 %) (Fig. 3).

Significant fractionation of paleoclimate-sensitive trace elements is observed. The Liushagang Formation demonstrates marked Sr depletion (mean = 112.48 ppm) relative to PAAS. The average Sr content decreases from 140.57 ppm in the Ls3 to 108.11 ppm in the Ls2 and 76.69 ppm in the Ls1. Conversely, Rb exhibits enrichment in the Ls2 (mean = 175.88 ppm) relative to the Ls3 (mean = 126.81 ppm) (Fig. 3).

4.2. Palynological records

A total of 36 palynological species were identified in the Liushagang Formation, including 8 fern, 5 gymnosperms, 21 angiosperms, and 2 algal species. Based on cluster analysis, three distinct palynological zones were identified, corresponding to three members respectively (Fig. 4).

4.2.1. Zone A (Ls3, early Eocene)

This zone was dominated by a high abundance of angiosperms (46.51 %) and a moderate abundance of algae (22.95 %) and gymnosperms (21.64 %), with negligible fern representation (8.90 %). The angiosperms were overwhelmingly dominated by subtropical and warm temperate broad-leaved trees, such as *Juglanspollenites* (15.36 %), *Quercoidites* (14.00 %), *Tricolpopollenite* (8.85 %), *Tricolporopollenites* (3.57 %), *Cupuliferoipollenites* (2.15 %), *Retitricolites* (0.74 %),

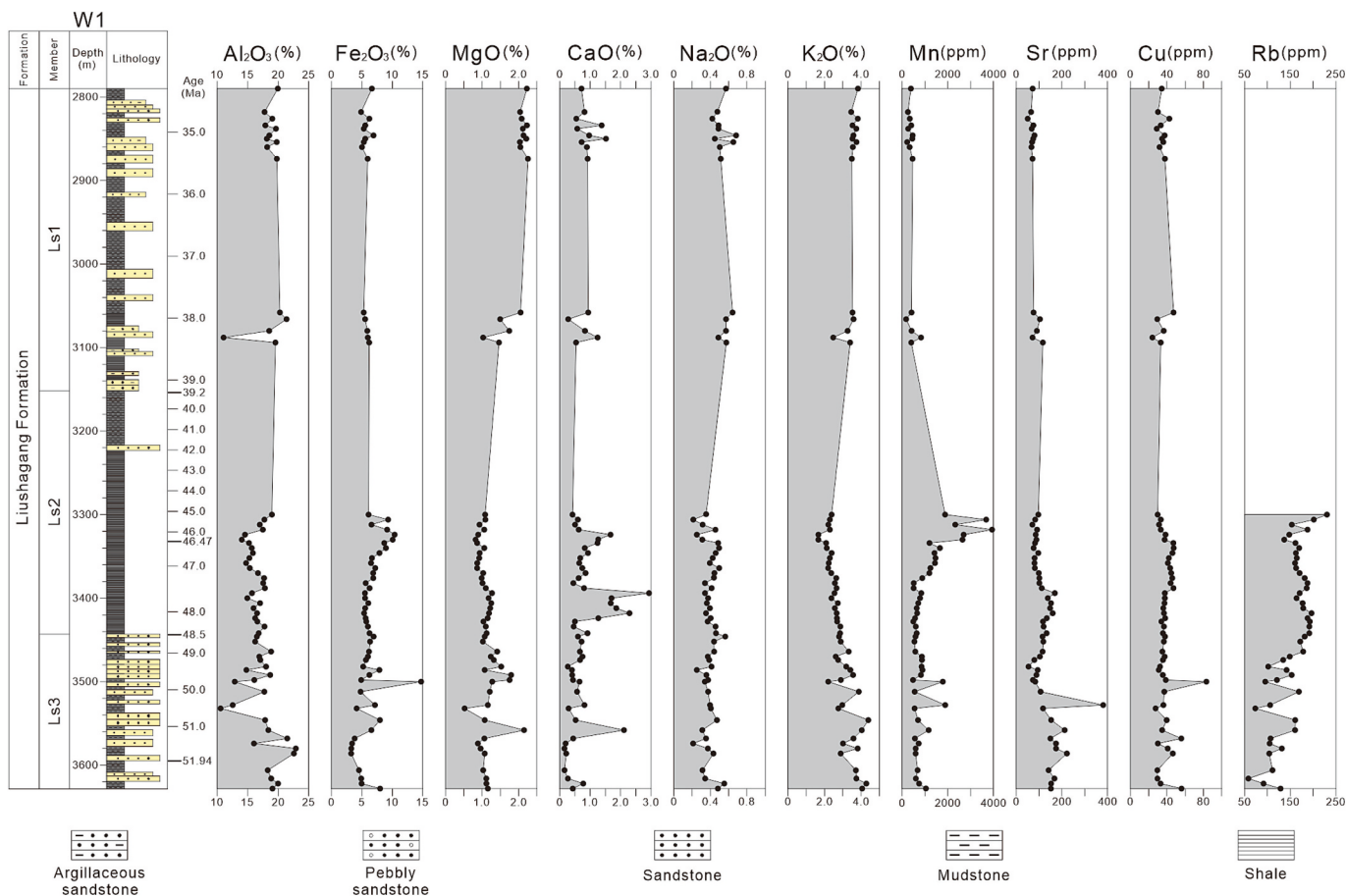


Fig. 3. Stratigraphic variation in abundances of partial major and trace elements of the Liushagang Formation from the borehole W1.

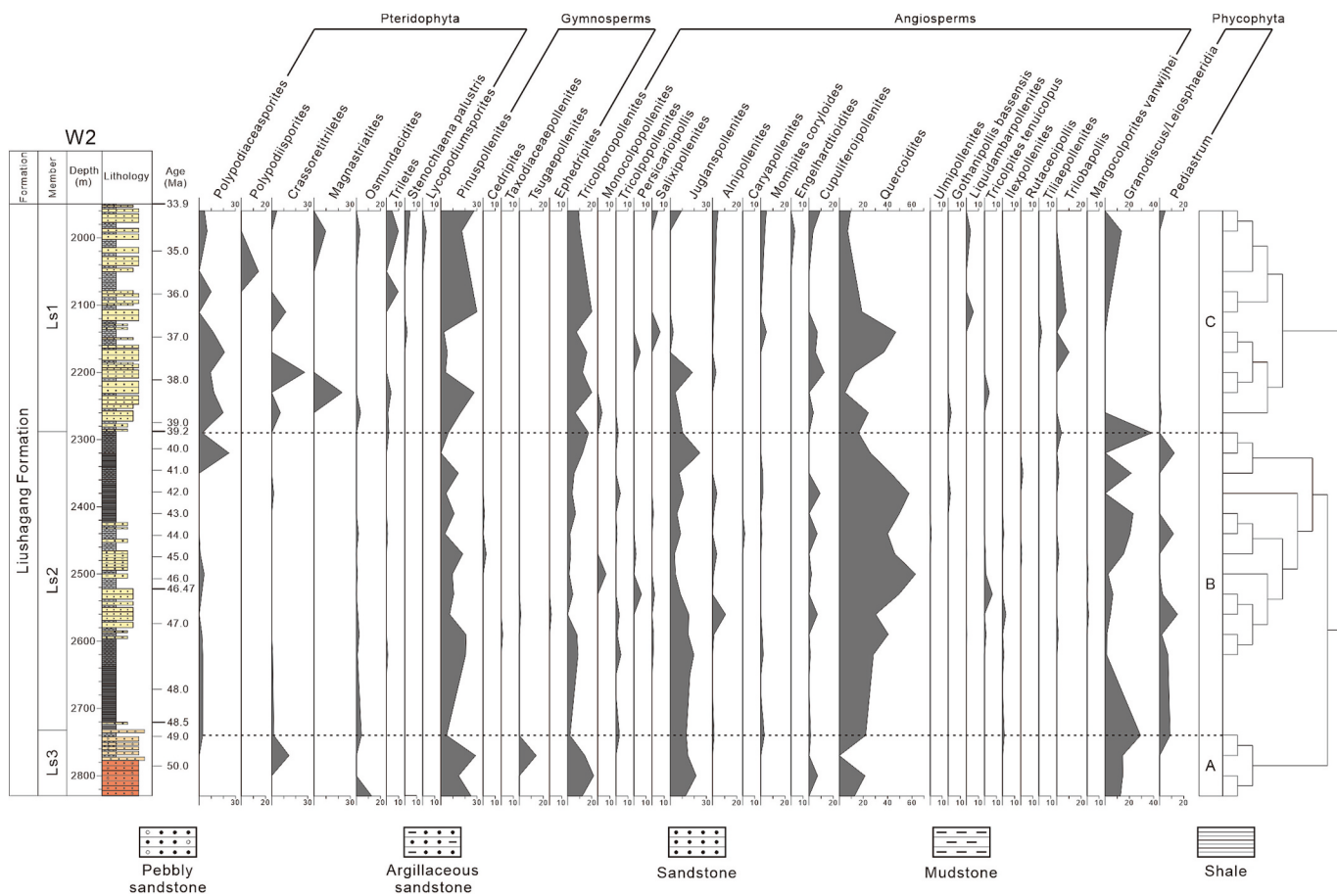


Fig. 4. Total pollen diagram and cluster analysis of the Eocene Liushagang Formation from the borehole W2.

Ilexpollenites (0.37 %), and *Alnipollenites* (0.37 %). Limited shrub components were represented solely by *Momipites coryloides* (7.4 %). Gymnosperms consisted of subtropical-temperate conifers: *Pinuspollenites* (18.07 %) and *Tsugaepollenites* (3.57 %). Algae formed a *Granodiscus/Leiosphaeridia* consortium (17.62 %) with minor *Bosedinia corrugis* (3.13 %) and *Pediastrum* (2.21 %). Fern diversity included *Osmundacidites* (4.23 %), *Crassoretitriletes* (3.94 %), *Polypodiaceaesporites* (0.37 %), and *Polypodiisporites* (0.37 %).

4.2.2. Zone B (Ls2, middle Eocene)

Compared with zone A, this zone was significantly reorganized. Angiosperms surged to 68.31 % dominance, while algae (15.92 %) and gymnosperms (10.93 %) declined significantly, accompanied by minimal fern presence (4.84 %). The angiosperm was overwhelmingly dominated by subtropical and warm temperate broad-leaved trees, featuring *Quercoidites* (40.44 %), *Juglanspollenites* (11.05 %), *Tricolpopollenite* (4.91 %), *Cupuliferoipollenites* (2.17 %), *Alnipollenites* (1.81 %), *Retitricolpites* (1.22 %), *Tricolporopollenites* (1.02 %), *Tricolpites tenuiculus* (0.93 %), and *Salixipollenites* (0.45 %). Shrubs remained sparse, comprising *Momipites coryloides* (0.83 %) and *Ephedripites* (0.12 %), while herbs included *Trilobapollis* (0.73 %) and *Persicarioipollis* (0.67 %). Gymnosperms transitioned to *Pinuspollenites* (10.28 %), *Cedripites* (0.31 %), *Tsugaepollenites* (0.12 %), and *Taxodiaceaepollenites* (0.10 %). Algae shifted to a *Granodiscus/Leiosphaeridia* consortium (11.15 %) with *Pediastrum* (4.15 %).

4.2.3. Zone C (Ls1, late Eocene)

Zone C recorded a pronounced resurgence of ferns (24.97 %) and drastic decline of algae (3.11 %), alongside angiosperm reduction (52.76 %) and gymnosperm recovery (19.16 %). The angiosperms

retained subtropical and warm temperate broad-leaved trees dominance, featuring *Quercoidites* (18.14 %), *Tricolpopollenites* (10.82 %), *Juglanspollenites* (6.16 %), *Cupuliferoipollenites* (4.09 %), *Tricolporopollenites* (1.66 %), and *Alnipollenites* (1.47 %). Shrubs were represented by *Momipites coryloides* (2.25 %), while herbs included *Trilobapollis* (3.28 %) and *Persicarioipollis* (0.53 %). Fern diversified significantly, comprising *Polypodiaceaesporites* (9.26 %), *Crassoretitriletes* (5.21 %), *Magnastriatites howardi* (3.60 %), *Triletes* (2.24 %), *Polypodiisporites* (1.43 %), *Stenochlaena palustris* (1.02 %), and *Osmundacidites* (0.71 %).

5. Discussion

5.1. Evolution of Eocene vegetation landscapes

Integrated analysis of Eocene palynological assemblages from the Weixinan Sag, combined with paleovegetation structure reconstruction based on plant ecological preferences, reveals a well-constrained paleoclimatic evolutionary trajectory. The palynological record demonstrates that the angiosperms were dominant in the Weixinan Sag, while the percentages of angiosperms, gymnosperms and ferns taxa show marked stratigraphic fluctuations (Fig. 5a). The vegetation profile comprised conifers, evergreen and deciduous broadleaf trees, shrubs, and herbs. Notably, subtropical and warm temperate broadleaf trees predominated overwhelmingly, such as *Quercus*, *Juglans*, Fagaceae, *Alnus*. Xerophilous taxa were conspicuously absent, such as *Ephedra*, Chenopodiaceae, *Artemisia* (Fig. 5b). This ecological configuration suggests the study area sustained a consistently warm-humid subtropical climate.

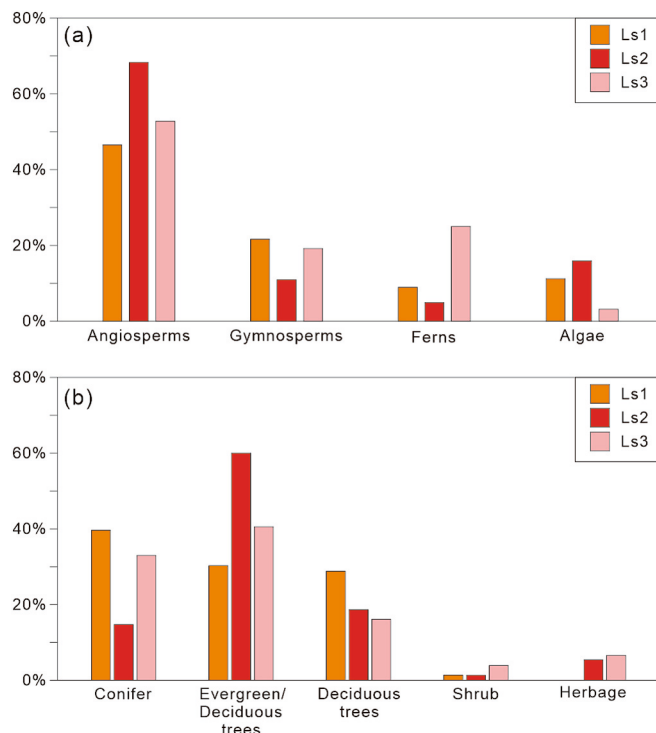


Fig. 5. Type and percentage of the Eocene Liushagang Formation. (a) Sporopollen types. (b) Plant types.

5.1.1. Early Eocene: vertical vegetation zonation and warm-humid climate

The early Eocene palynoflora was of low taxonomic diversity, dominated by broadleaf and coniferous trees, mainly hygrophytic and mesophytic vegetation. The algae were the most prosperous, while ferns remained minimally developed. The following phytocoenotic combinations were present: (1) hygromesophytic forest palaeocoenoses including *Juglans*, *Quercus*, *Castanea*, *Alnus*, and *Ilex*; (2) hygrophilic and cold-resistant forest palaeocoenoses with *Pinus*; (3) hygrophytic to hygrophytic swampy palaeocoenoses containing the genera *Granodiscus*, *Leiosphaeridia*, *Pediastrum*, and *Bosedinia corrugis*; (4) hygrophytic undergrowth palaeocoenoses with the genera *Osmundacitides*, and *Crassoretitritiletes*. The coexistence of thermophilic-hygrophilic taxa (e.g., *Juglans*, *Quercus*) and cold-resistant conifers (e.g., *Pinus*) suggests pronounced vertical vegetation zonation, likely driven by climatic altitudinal gradients. Conifers such as *Pinus* probably flourished on the highlands surrounding the basin.

This ecosystem configuration parallels modern northern subtropical monsoon biomes, indicative of a warm-humid climate. It provided hydro-thermal conditions for proliferation of broadleaf forests and lacustrine algae. During this interval, lacustrine systems sustained prolific algal proliferation. The surrounding flatlands were dominated by subtropical deciduous broad-leaved forests primarily composed of *Juglans* and *Quercus*, while *Alnus*-rich wetland communities thriving in hydromorphic habitats. The highland supported coniferous forests adapted to cool-humid conditions (Fig. 6c).

5.1.2. Middle Eocene: Conifers recession and humidification

Marked ecological reorganization occurred in the middle Eocene. The flora comprised a mixture of evergreen, deciduous and coniferous plants, characterized by significantly enhanced vegetation diversity and pronounced tropicalization of the flora compared to the early Eocene. The abundance of hermaphyllous and evergreen/deciduous elements (e.g., *Quercus*, *Alnus*, *Salix*) increased, while mesophytic and conifers diminished (e.g., *Juglans*, *Pinus*). In addition, the shrub and herbaceous representation were suppressed.

It reflects enhanced hydrothermal conditions and strengthened seasonality. Lowland vegetation transitioned from deciduous to evergreen-deciduous broadleaf forests, with high canopy density limiting under-story growth. Concurrently, reduced coniferous proportions (e.g., *Pinus*) suggest the retreat of conifer forests to higher elevations, while mountain around the study area evolved into mixed forests (Fig. 6b).

5.1.3. Late Eocene: Fern proliferation and aridification

The most distinctive feature of palynofloral assemblage was the near disappearance of algae (e.g., *Granodiscus*, *Leiosphaeridia*, *Pediastrum*, *Bosedinia corrugis*) and significant increase of ferns (e.g., *Polypodiodes*, *Crassoretitritiletes*). Ferns represented by *Polypodiodes* grew in the shade of trees, shrubs or valleys. The marked increase in ferns reflects reduced forest canopy density resulted in the formation of fern-dominated ground cover layers in forest gap areas. The evergreen and deciduous broadleaf trees remained dominant, while hygrothermal components (e.g., *Quercus*, *Juglans*, *Alnus*, *Hamamelidaceae*, *Ulmus*) declined. The abundance of confers increased and *Pinus* re-emerged as a dominant genus.

The landscape suggested a cooling and aridification trend as a response to global drop in temperature in the late Eocene. Frens grew under sparse evergreen-deciduous broadleaf forests with dramatic reductions in lacustrine algae. Mountains underwent reverse succession, being recolonized by coniferous forests (Fig. 6a).

5.2. Eocene paleoclimatic evolution in the Weixinan Sag

The chemical weathering in source areas is intensified under humid climatic conditions, causing in difference in elements of sedimentary rock (Zeng et al., 2022). Mobile elements (e.g., Na, K, Ca, Mg) are preferentially leached, transported, and deposited, while stable elements (e.g., Al, Ti, Sc, Zr, Hf, Th, Y, REEs) become residually enriched in weathering crusts (Lerman, 1978). This systematic elemental fractionation provides critical evidence for quantitatively characterizing weathering processes. Therefore, some geochemical proxies are often used to analyze the paleo-climate characteristics, such as the chemical alteration index (CIA), climate index (CI), index of compositional variability (ICV), weathering index of parker (WIP), K_2O/Al_2O_3 , Mg/Ca , and Rb/Sr (Nesbit and Young, 1982; Cao et al., 2012; Roy and Roser, 2013; Omietimi et al., 2022; Huang et al., 2024; Algeo et al., 2025).

As the most widely used tool for evaluating chemical weathering patterns in sediments, the CIA and ACNK ternary diagrams can effectively trace weathering pathways and intensities. The calculation formula is: $CIA = [Al_2O_3 / (Al_2O_3 + CaO^* + Na_2O + K_2O)] \times 100$, where CaO^* is the silicate fraction CaO content, and oxides are expressed as molar proportions. As can be seen from Fig. 7, the CIA value of the Liushagang Formation range from 71.92 to 84.88 (mean = 78.97) with 71.92–84.32 (avg. 78.19) in the Ls3, 78.48–84.88 (avg. 80.87) in the Ls2, and 72.06–80.27 (avg. 76.99) in the Ls1 (Fig. 7). According to classification criteria published by Nesbitt and Young (Nesbit and Young, 1982), CIA value of 50–60 represents weak chemical weathering, with 60–80 suggesting moderate chemical weathering, 80–100 indicating strong chemical weathering. This shows moderate to strong chemical weathering in the Weixinan Sag during the Eocene. Among them, it suffered from strong chemical weathering in the middle Eocene and moderate chemical weathering in the early and late Eocene. In addition, the weathering trend demonstrates that the parent rocks are predominantly granitic, with sediments clustering near the A-K axis. $CaO + Na_2O$ have been largely leached, and K-feldspar has completely decomposed into illite-muscovite assemblages. Compared to Ls3 and Ls1, Ls2 samples shift closer to the A apex and transit toward kaolinite and/or gibbsite, while reflects stronger weathering and wetter climate.

The diagram of CIA vs. CI indicates semi-humid to humid conditions in study area during the Eocene (Fig. 8a). The CI value (C-value) captures paleoclimatic information through ratios of mobile to stable elements and its calculation formula is: $CI = (Fe + Mn + Cr + Ni + V + Co)$

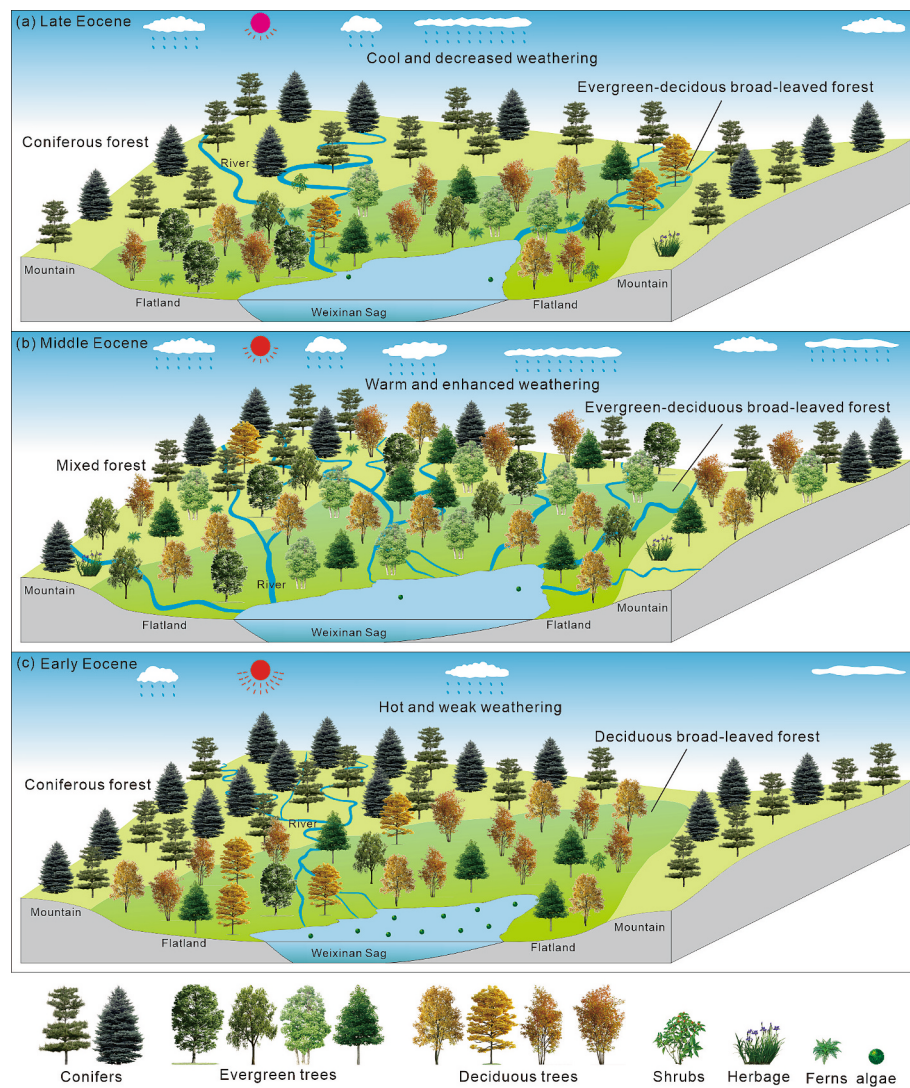


Fig. 6. The vegetation landscapes (terrestrial ecosystems) of the Weixinan Sag. (a) Late Eocene. (b) Middle Eocene. (c) Early Eocene.

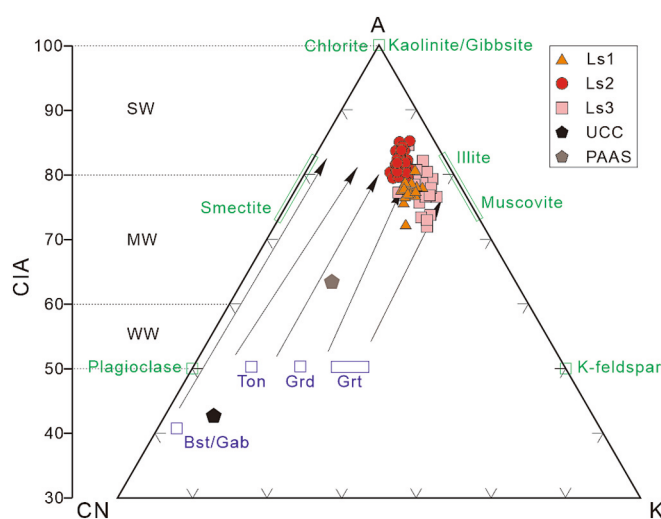


Fig. 7. The A-CN-K diagram for weathering of the Liushagang Formation.

/ (Ca + Mg + K + Na + Sr + Ba). A humid environment is indicated by a high C-value, with C-values >0.8 indicating humid conditions, 0.6–0.8 suggesting semi-humid conditions, 0.4–0.6 indicating semi-humid to semi-arid conditions, 0.2–0.4 indicating semi-arid conditions, and C-values <0.2 indicating arid conditions (Omietimi et al., 2022). The diagram reflects the Weixinan Sag was under a humid climate during the middle Eocene and a semi-humid climate during the early and late Eocene. Compared with Ls3 and Ls1, the samples from Ls2 exhibit higher average CIA values and CI values. The average C-value of Ls3, Ls2, and Ls1 are 0.97, 1.38, and 0.80, respectively.

The diagram of CIA vs. ICV suggests the samples from the Liushagang Formation experienced intense weathering and long-distance transport under humid climatic conditions (Fig. 8b). Under humid climatic conditions, the combined effects of intense weathering and long-distance transport significantly enhance the compositional maturity of sediments, which is commonly characterized by ICV. It was computed using the equation: $ICV = (Fe_2O_3 + K_2O + Na_2O + CaO + MgO + TiO_2) / Al_2O_3$. A higher compositional maturity corresponds to a lower ICV value, and ICV value <1 typically implies the existence of mature sediments (Omietimi et al., 2022). The plots show that the ICV values of the Liushagang Formation samples range from 0.46 to 1.31 (mean = 0.76), demonstrating sediments with relatively high compositional maturity. Compared to Ls1 and Ls3, samples from Ls2 exhibit higher average CIA values and lower average ICV values, indicating a greater degree of

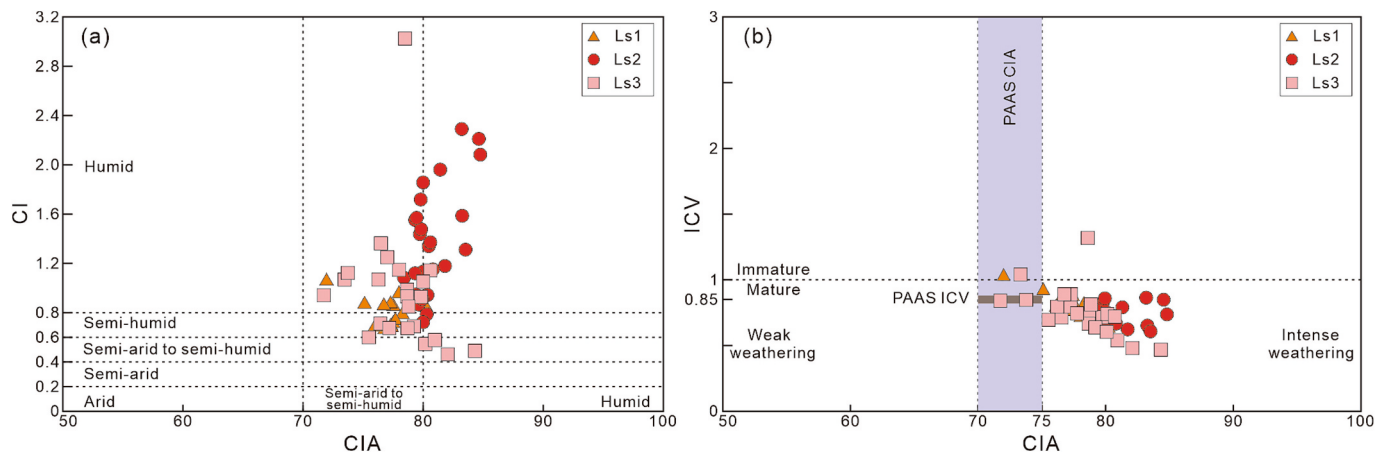


Fig. 8. The CIA vs. CI and CIA vs. ICV diagram for weathering and paleoclimate of the Liushagang Formation.

overall weathering and higher rainfall.

The results are supported by other proxies, including WIP value, K_2O/Al_2O_3 ratio, Mg/Ca ratio, Rb/Sr ratio. WIP value, K_2O/Al_2O_3 ratio, Mg/Ca ratio correlate negatively with precipitation, while Rb/Sr ratio shows positive correlation (Omietimi et al., 2022; Huang et al., 2024). The Ls3 samples exhibit high WIP value (27.09–48.55, average = 36.68), K_2O/Al_2O_3 ratio (0.13–0.26, average = 0.19), Mg/Ca ratio (0.86–5.43, average = 2.56) and low Rb/Sr ratio (0.28–1.89, average = 1.08). In contrast, the Ls2 samples have lower WIP value (22.55–35.78,

average = 29.54), K_2O/Al_2O_3 ratio (0.11–0.17, average = 0.15), Mg/Ca ratio (0.45–2.17, average = 1.10) and higher Rb/Sr ratio (1.16–2.40, average = 1.71). The Ls1 sample shows high WIP value (31.55–45.76, average = 42.32), K_2O/Al_2O_3 ratio (0.17–0.22, average = 0.19), Mg/Ca ratio (0.70–3.23, average = 2.20) (Fig. 9). Furthermore, it is notable that during the early Eocene, a peak in humidity occurred around 51–53 Ma, indicating the presence of intense rainfall events likely associated with the Early Eocene Climatic Optimum (EECO). During the EECO, atmospheric CO_2 concentrations were estimated to range between 600 and

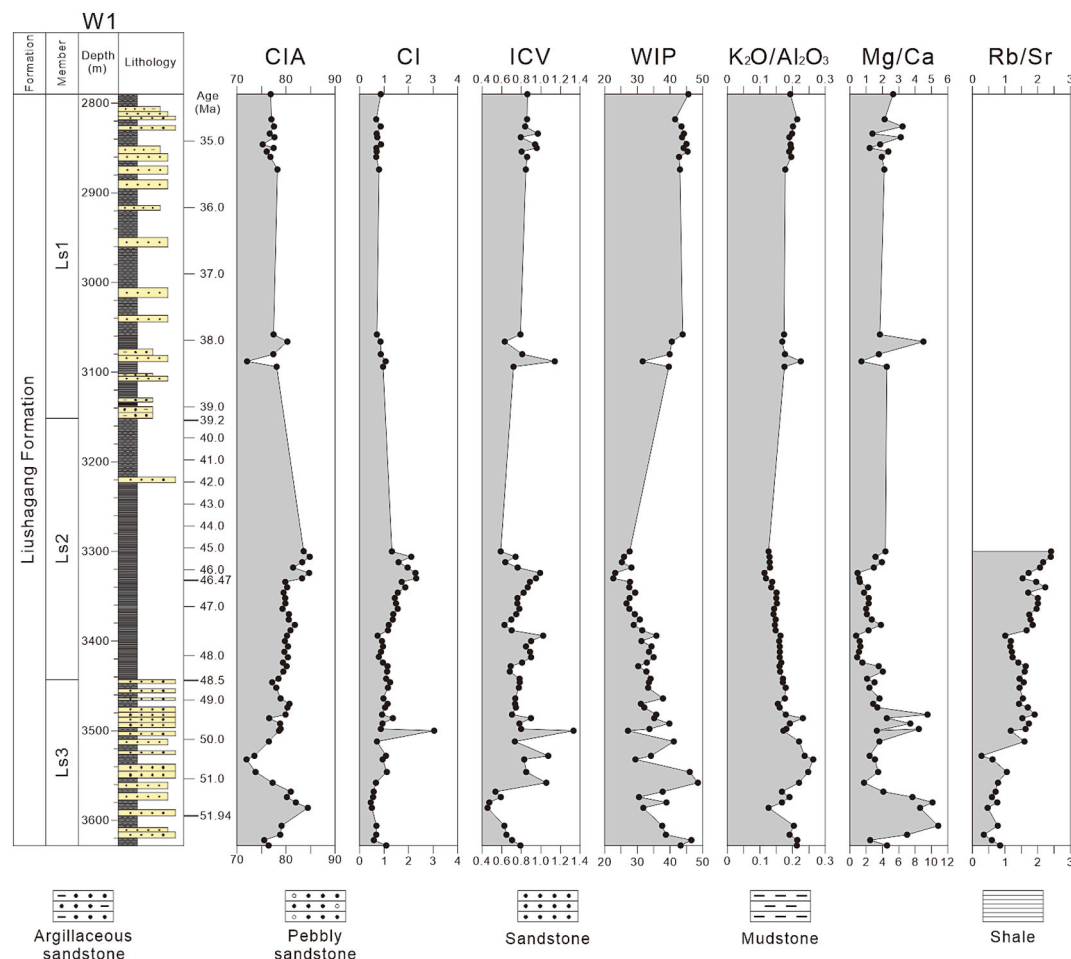


Fig. 9. Stratigraphic variation in CIA, CI, ICV, WIP, K_2O/Al_2O_3 , Mg/Ca, Rb/Sr.

2000 ppm, with global mean temperature approximately 13 ± 2.6 °C higher than present-day levels (Zachos et al., 2001; Huber and Caballero, 2011; Burke et al., 2018). Under these enhanced wetter conditions, the Weixinan Sag experienced substantially increased rainfall, promoting intense chemical weathering.

5.3. Mechanisms driving eocene climatic evolution

5.3.1. Monsoonal circulation controlled Eocene Climate in the Weixinan Sag

Integrated analysis of paleoclimatic proxies and palynological records reveals that the Eocene climate of the Weixinan Sag maintained warm and humid characteristics with paleovegetation landscapes resembling the modern subtropical monsoon zones. It is noteworthy that the study region exhibited phased climatic evolution, characterized by intense rainfall during the EECO and subsequent weakened precipitation. The middle Eocene was marked by significantly enhanced rainfall, followed by late Eocene cooling-aridification. Although the Eocene globe underwent multiple short-term warming events, its long-term trend featured progressive cooling (Zachos et al., 2001; Pearson et al., 2007; Zachos et al., 2008). This regional trajectory contrasts with the globally dominant progressive cooling trend of the Eocene, underscoring the predominance of local climatic drivers over rainfall patterns.

The emergence and intensification of monsoonal atmospheric circulation during the Eocene might be a critical reason for driving the regional climatic evolution. Monsoonal atmospheric circulation can be defined as thermally driven circulations generating extreme seasonal precipitation contrasts, characterized by a hot-humid summer and cold-dry winter (Huber and Goldner, 2012; Licht et al., 2014). Another feature is recurrent dry-wet alternations across geological timescales (Wang, 2005). Palynological assemblages indicate that the early Eocene ecosystem in the study area was dominated by evergreen and deciduous trees, with co-occurrence of hygrophilous and mesophytic plants, and exhibited altitudinal vegetation zonation. This paleovegetation type resembles that of the modern monsoon region in southern China, characteristic of a humid subtropical climate with pronounced seasonal rainfall. Additionally, CIA, CI, ICV, WIP, K_2O/Al_2O_3 , Mg/Ca, and Rb/Sr values suggest a humid climate with recurrent climatic fluctuations. These features collectively suggest that a monsoon system, analogous to contemporary configurations, had extended into the northern South China Sea during the early Eocene.

Potential drivers include the seasonal migration of the Intertropical Convergence Zone (ITCZ) and the formation of the EASM. The ITCZ is primarily characterized by meridional oscillation, whereas EASM moisture transport exhibits a distinct zonal orientation. Integrated petrological, geochemical, and palynological evidence indicates that seasonal monsoon rainfall was widespread during the early Eocene in southern Tibet, the Nangqian Basin, the Gonjo Basin, and the northern South China Sea (Ding et al., 2017; Wang, 2022; Guan, 2021). This implies the existence of an approximately east-west oriented humid climatic zone controlled by the ITCZ across East Asia low-latitude regions. However, compared to inland basins, which recorded alternating humid and dry cycles, the northern South China Sea appears to have experienced a more consistently humid climate with fewer aridity indicators, suggesting higher regional precipitation. This east-west climatic contrast was especially evident in mid-latitude regions: deciduous broadleaf forests thrived in eastern coastal areas such as the Lufeng Sag and Taihei Sag, whereas central China was dominated by arid desert vegetation (Zhang et al., 1990; Li, 1998; Xie et al., 2022).

The emergence of the EASM offers a compelling explanation for this phenomenon. Although scholarly consensus remains elusive regarding primary drivers of the EASM, multidisciplinary paleoclimatic proxies highlight a structural reorganization of EASM during the middle Eocene, widely regarded as a critical juncture for the establishment of the modern East Asian monsoon system (Quan et al., 2012b; Wang et al., 2013; Xie et al., 2019; Ma et al., 2019; Tardif et al., 2020; Song et al.,

2023; Kong et al., 2024; Cai and Kong, 2024). However, a non-monsoon-dominated climate does not mean that monsoon circulation completely disappeared, but indicates a mean climate state without monsoon playing a dominant role for a long period (Zhang et al., 2012). This paradigm shift necessitates reinterpretation of early Eocene climatic archives. Under the high-temperature conditions and paleogeographic setting of the early Eocene, a relatively weak land-sea thermal contrasts may have supported the development of weak monsoonal circulations in parts of East Asia. Particularly within East Asian low-latitude paralic belts, amplified diurnal temperature gradients between terrestrial and marine realms likely potentiated proto-monsoonal dynamics through enhanced sea breeze-land breeze oscillations - a precursor mechanism to full development of the EASM. Numerical simulations corroborate that even under reduced hemispheric thermal contrasts characteristic of early Paleogene hothouse climates, such localized thermodynamic imbalances could sustain weak but climatically significant moisture recycling patterns, effectively bridging the conceptual gap between modern monsoonal vigor and putative monsoon-absent paleoclimate states (Zhang et al., 2012; Zoura et al., 2020).

Overall, during the early Eocene, the Weixinan Sag was influenced by both the seasonal migration of the ITCZ and weak monsoonal circulation associated with the EASM, supporting vegetation communities analogous to those found in modern monsoon regions. A vertically stratified subtropical forest developed, characterized by floodplain deciduous broadleaved forests and montane coniferous forests exhibiting clear altitudinal zonation, alongside hygrophilous and mesophytic tree taxa. Similar climatic patterns have been documented in the Pearl River Mouth Basin, where evergreen-deciduous broadleaved forests—dominated by *Quercus*, *Alnus*, and *Fraxinus*—flourished in the Lufeng Sag (Li, 1998). By the middle Eocene, chemical weathering intensity in the Weixinan Sag increased significantly, coinciding with a notable rise in tropical-subtropical floral elements and the expansion of broadleaved forests, indicative of enhanced seasonality. This period aligns with climatic shifts recorded in the Jianghan and Qingjiang Basins, and stands in sharp contrast to contemporaneous aridification in southwestern China, suggesting the emergence of a regional East Asian Summer Monsoon regime (Tong et al., 2001; Wang et al., 2013; Wang, 2019; Fang et al., 2021; Xie et al., 2022). During this phase, more extensive and intensified monsoonal circulation delivered substantial rainfall to the Weixinan Sag, while the influence of the ITCZ markedly diminished. In the late Eocene, weathering intensity in the area declined, as evidenced by an increase in fern spores and deciduous components, reflecting decreased precipitation and lower temperatures potentially linked to global cooling. Collectively, these findings illustrate that early Eocene low-latitude regions experienced local sea-land breeze systems, initially driven by thermal contrast mechanisms along coastlines under globally elevated temperatures.

5.3.2. Variability in the intensity of the EASM

To understand the spatial extent and intensity of the EASM during the Eocene, this study compared the Weixinan Sag with 49 Eocene palynological records across East Asia. On this basis, we reconstruct vegetational clusters and evaluate climatic aridity-humidity shifts through systematic analysis of floras (Table 1). During the Eocene, the flora of East Asia included evergreen broad-leaved forests (EBF), evergreen deciduous broad-leaved forests (EDBF), deciduous broad-leaved forests (DBF), broad-leaved coniferous mixed forests (MF), coniferous forests (CF), and sparse-wood shrubs (SWS) (Li et al., 2022). Spatial phytogeographic patterns reveal coherent biogeographic provinces, effectively mapping the Eocene EASM's operative range and intensity gradients. Particularly significant are distributional discontinuities in *Ephedra*-*Zygophyllaceae* dominated steppe communities versus broadleaf forest domains, demarcating the monsoon's northern penetration limits and continental interior aridity cores.

Reconstruction outcomes delineate an expansive zonal aridity corridor dominated by desert ecosystem across mid-latitude East Asia

Table 1

Eocene pollen sampling sites and corresponding vegetation types. EBF: evergreen broad-leaved forests; EDBF: evergreen deciduous broad-leaved forests; DBF: deciduous broad-leaved forests; MF: broad-leaved coniferous mixed forests; CF: coniferous forests; SWS: sparse-wood shrubs.

Site	Location	Coordinate	Paleoclimate records			Reference
			Early Eocene	Middle Eocene	Late Eocene	
1	Changchang Basin	110.3°E, 19.4°N	EDBF	EDBF	EDBF	Yao, 2006; Xie et al., 2019
2	Zhangjiang Sag, Beibowan Basin	110.03°E, 20.55°N		EDBF	EDBF	Zhang, 1981
3	Weixinan Sag, Beibowan Basin	108.57°E, 20.37°N	DBF	EDBF	EDBF	This study
4	Haizhong Sag, Beibowan Basin	108.30°E, 20.26°N		EDBF	EDBF	Luo et al., 2013
5	Hepu Basin	108.57°E, 20.37°N		EDBF	EDBF	Yang, 1996
6	Maoming Basin	110.8°E, 21.5°N		EDBF		Xie et al., 2019
7	Lufeng Sag, Pearl River Mouth Basin	113.3°E, 41.7°N	EDBF	EDBF	EDBF	Li, 1998
8	Ningming Basin	107.02°E, 22.6°N			MF	Wang et al., 2003
9	Baise Basin	106.6°E, 23.9°N		EDBF		Xie et al., 2019
10	Puyang Basin	105.16°E, 23.28°N			CF	Yang, 2022
11	Lvhe Basin	105.21°E, 25.10°N			MF	Liu, 2019
12	Jianchuan Basin	99.54°E, 26.32°N			MF	Wu, 2017
13	Markam Basin	98.36°E, 29.41°N			EDBF	Chen et al., 2021
14	Shalmu Basin	98.06°E, 32.58°N	SWS	SWS	SWS	Wei and Luo, 2005
15	Nangqian Basin	96.29°E, 32.12°N			SWS	Yuan et al., 2020
16	Lunpola Basin	88.46°E, 30.58°N		EBF	EBF	Wang et al., 1975
17	Qianjiang Sag, Jianghan Basin	112.8°E, 30.4°N		DBF	DBF	Tong et al., 2001
18	Qingjiang Basin	116.1°E, 27.9°N	SWS		DBF	Xie et al., 2022
19	Nanling Basin	118.26°E, 31.17°N	DBF		DBF	Zhang et al., 1986
20	Xuanzhou Basin	118.7°E, 30.9°N		DBF		Li, 2005
21	Taibei Sag, East China Sea Shelf Basin	121.7°E, 26.4°N	DBF	DBF	DBF	Zhang et al., 1990
22	Xihu Sag, East China Sea Shelf Basin	119.16°E, 29.36°N		DBF	DBF	Zhang, 2015; Li et al., 2024
23	Gaoyou Sag, South Yellow Sea Basin	119.4°E, 32.8°N	DBF	DBF	DBF	Zhang and Qian, 1992
24	Tantou Basin	111.6°E, 33.8°N	MF	DBF	DBF	Wang et al., 1984; Su, 2022
25	Lushi Basin	111.05°E, 34.05°N		DBF	DBF	Yang et al., 2005
26	Lingbao Basin	110.8°E, 34.5°N	DBF		DBF	Sun, 1984
27	Weihe Basin	109.31°E, 34.19°N		DBF	DBF	Han, 2023
28	Tongxin Basin	105.96°E, 37.11°N			SWS	Song et al., 2008
29	Lanzhou Basin	103.35°E, 36.17°N			SWS	Song et al., 2008
30	Xining-Minhe Basin	101.77°E, 36.62°N		DBF	SWS	Sun et al., 1985; Wang et al., 1986; Song et al., 2008
31	Minhe Basin	102.4°E, 36.2°E			SWS	Yu et al., 2003
32	Xining Basin	101.47°E, 36.31°N			SWS	Zhao et al., 2015
33	Qaidam Basin	95.26°E, 37.24°N	DBF	SWS	SWS	Song et al., 2008; Lu et al., 2020
34	Hoh Xil Basin	92.55°E, 34.27°N			SWS	Miao et al., 2016
35	Jiuquan Basin	97.02°E, 40.17°N			SWS	Miao et al., 2008
36	Turpan-Hami Basin	90.08°E, 42.54°N	DBF	SWS	SWS	Song et al., 2008
37	Shache Depression, Tarim Basin	77.3°E, 38.3°N	DBF	DBF	SWS	Zhao et al., 1982; Wang et al., 1986
38	Junggar Basin	87.45°E, 45.39°N	DBF	DBF	SWS	Song et al., 2008
39	Kuqa Depression, Tarim Basin	82.9°E, 41.7°N	DBF	DBF	SWS	Zhao et al., 1982; Wang et al., 1986
40	Otog, Ordos Basin	107.29°E, 38.11°N	SWS	SWS	SWS	Song and Zhang, 1990
41	Yunsi-Wenkou-Tailai Sag	116.04°E, 35.35°N		DBF	DBF	Tong, 1989
42	Changle Sag	118.55°E, 36.43°N		DBF	DBF	Wang, 2005
43	Dongying Sag, Bohai Bay Basin	118.25°E, 37.15°N	MF	DBF	DBF	Peng, 2021
44	Nanpu Sag, Bohai Bay Basin	118.30°E, 39.20°N		DBF	DBF	Xia et al., 2015
45	Huanghua Sag, Bohai Bay Basin	117.27°E, 38.29°N		MF	MF	Zhang and Yin, 2005
46	Fushun Basin	123.9°E, 41.8°N	MF	MF	MF	Shi et al., 2008; Han and Shu, 2020; Wei et al., 2021; Li et al., 2022
47	Huadian Basin	126.43°E, 42.56°N		MF	MF	Meng et al., 2018
48	Wancan Basin	125.53°E, 43.46°N	MF	MF	MF	Zhang et al., 2010
49	Hunchun Basin	130.5°E, 42.7°N	MF	MF	MF	Wang et al., 1986; Zhang et al., 1986; Wang, 2003
50	Yilan Basin	129.3°E, 46.1°N	MF	MF	MF	He and Tao, 1997

during the early Eocene, aligning with prior continental-scale reconstructions ([Sun and Wang, 2005](#); [Quan et al., 2012b](#); [Li et al., 2022](#); [Song et al., 2023](#)). Yet we find that the arid belt was confined to continental interiors, while some contemporaneous coastal basins (e.g.,

Nanling Basin, East China Sea Basin, Yellow Sea Basin) exhibited warm-humid climates supporting deciduous or mixed forests with evergreen components ([Zhang et al., 1986](#); [Zhang et al., 1990](#); [Zhang and Qian, 1992](#)). The pronounced humidity gradient from eastern littoral zones to

western hinterlands reveals limited marine moisture penetration restricted to coastal regions. The pattern is more obvious in low latitudes, manifested through sharp phytogeographic transitions from tropical-subtropical evergreen-deciduous broad-leaved forests along eastern coastlines through westwards-degrading deciduous broad-leaved forests with escalating xerophytic components. These changes in rainfall, particularly evidenced by the stark low-latitude precipitation gradient, fundamentally challenges conventional models of Eocene East Asian climate uniformity. Weak diurnal sea-land thermal circulations along coastlines were able to maintain weak sea-land breezes without sustaining continent-scale moisture transport, resulting in localized humidity pockets, particularly in low latitudes (Fig. 10c).

Pivotal climatic reorganization occurred in the middle Eocene. The inland desert scrub was replaced by deciduous forests and mixed forests, while evergreen deciduous broad-leaved forest expanded in coastal areas, with increasing evergreen broad-leaved components and reduced conifer representation. This phytogeographic restructuring manifested enhanced regional humidity, with low-latitude littoral zones dominated by luxuriant evergreen broadleaved communities transitioning northwestward through evergreen-deciduous ecotones into deciduous woodlands before terminating in residual desert scrub. The spatial progression reflected enhanced regional rainfall and emerging coastal-inland humidity contrasts, marking the formal establishment of the East Asian monsoon system. Concurrent sedimentary and geochemical archives capture this hydrological transformation: (1) deep lacustrine shales in the Beibuwan Basin and Pearl River Mouth Basin, contrast with rhythmic salt-mudstone sequences in the Jianghan Basin, and distinctive red beds and gypsum layers in the Xining Basin (Sayem et al., 2018; Peng et al., 2023; Cai and Kong, 2024; Liu et al., 2025); (2) Strong weathering in the southeast, moderate in the middle, and weak in the northwest (Sayem et al., 2018; Wang et al., 2022; Wang, 2022; Peng et al., 2023). The synchronicity between evergreen forest expansion in paralic regions, interior desert contraction, and weathering intensity zonation provides diagnostic evidence for monsoon establishment, reflecting the integration of previously fragmented moisture transport mechanisms into a coherent atmospheric circulation system capable of sustaining regional-scale humidity gradients - a climatic threshold crossed during middle Eocene reorganization of Asian terrestrial environments (Fig. 10b).

The late Eocene vegetation configuration largely perpetuated middle Eocene phytogeographic patterns while exhibiting progressive xerophytic intensification, marked by expanding arid-adapted taxa and coniferous proliferation. Regional manifestations mainly included: (1) deciduous arboreal dominance amplified in southeastern basins (Maoming, Beibuwan, Pearl River Mouth, Ningming, etc.) (Li, 1998; Aleksandrova et al., 2015; Herman et al., 2017); (2) xerophytic herb-shrub communities proliferated in the central and East China basins (East China Sea Shelf, South Yellow Sea, etc.) (Zhang et al., 1990; Zhang and Qian, 1992); (3) ecological simplification from mixed forests to shrubs in northwestern interior basins (Xining, Minhe, etc.) (Yu et al., 2003; Song et al., 2008; Hoorn et al., 2012; Zhao et al., 2015). Additionally, the Tarim Basin became fully arid, with vegetation transitioning from mixed and deciduous forests to desert and shrubs dominated by Zygophyllaceae and *Ephedra*, which may relate to the retreat of the Paratethys Sea. This broader patterns of coniferous expansion and deciduous persistence, illustrate the late Eocene's climatic duality: general cooling and drying caused by the decline of atmospheric pCO_2 led to the weakening of the EASM although the retreat of the Paratethys Sea strengthened the land-sea thermal contrast (Fig. 10a).

Paleovegetation reconstructions unveil a three-phase evolutionary model for the Eocene East Asian monsoon system. During the early Eocene, incipient monsoonal dynamics manifested as thermally-driven coastal breeze systems, where amplified diurnal land-sea temperature differentials – particularly under rapid continental heating cycles – generated localized low-pressure cells capable of drawing limited maritime moisture inland, sustaining narrow humidity corridors

without continental-scale penetration. During the middle Eocene, monsoon intensification marked a regime shift, likely driven by incipient uplift phases of the Tibetan Plateau that amplified seasonal landmass thermal inertia, thereby restructuring atmospheric pressure gradients to enable deep monsoon penetration into continental interiors through established moisture conveyor systems - a transformation permanently altering Asia's hydrological architecture. By the late Eocene, Paradoxically, monsoon attenuation occurred despite enhanced land-ocean thermal contrasts following the Tarim Sea's retreat, revealing the overriding influence of global cooling trends: declining temperatures suppressed evaporation-precipitation recycling efficiency while reducing atmospheric moisture-holding capacity, effectively counteracting potential monsoon intensification from paleogeographic boundary conditions. This tripartite evolutionary sequence demonstrates the interaction between tectonic forcing and global thermal states in monsoon development, where greenhouse climate provided necessary conditions for sustained monsoonal circulations and plateau orogeny expanded this advantage. Crucially, the early Eocene coastal breeze prototypes established the blueprint for subsequent monsoon systems, while middle Eocene tectonic-climatic synergy enabled true monsoonal emergence through combined landmass elevation and preserved greenhouse conditions, ultimately culminating in late Eocene climatic decay as cooling overwhelmed regional thermodynamic disequilibrium states.

6. Conclusion

Integrative analysis of Pollen assemblages and geochemical proxies in the Weixinan Sag delineates a dynamic Eocene climatic regime oscillating between humid subtropical conditions and seasonal aridity, underpinned by monsoonal atmospheric reorganization. Three evolutionary phases are resolved: (1) early Eocene (55.8–48.5 Ma) ecosystems sustained deciduous broadleaved lowland forests and montane conifers under moderate to intense humidity, transitioning from seasonal intense precipitation during the EECO toward weaker rainfall; (2) middle Eocene (48.5–39.2 Ma) climatic optimum drove forest reorganization through intensified humidity, manifested as lowland evergreen-deciduous broadleaved communities and altitudinal conifer-broadleaf ecotones alongside peak weathering intensities, signaling monsoon-moderated seasonality; (3) late Eocene (39.2–33.9 Ma) cooling-aridification triggered fern proliferation and coniferous resurgence under weakened weathering.

Paleovegetation landscapes similar to the modern monsoon region and chemical weathering intensity, marked by seasonal precipitation fluctuations, confirms operational monsoonal circulation since the early Eocene, predating previous estimates. Regional synthesis reveals a trajectory of EASM: proto-monsoonal cells initiated in early Eocene low-latitude coastal areas through greenhouse-enhanced land-sea thermal gradients, matured into a continental-scale system during middle Eocene paleogeographic restructuring, then attenuated in late Eocene despite persistent thermal contrasts as global cooling overrode paleogeographic changes on the effects of thermal gradients. Crucially, middle Eocene monsoon intensification coincided with coeval biotic turnovers across East Asia, demonstrating tectonic-climatic coupling in reshaping the region's hydroclimatic architecture. These findings recalibrate the Eocene Asian monsoon's developmental chronology, emphasizing its early Eocene coastal origins, middle Eocene continentalization, and late Eocene sensitivity to global thermal states.

Availability of data and materials

The research data of this study are given in the additional tables and can be obtained by requesting the corresponding author.

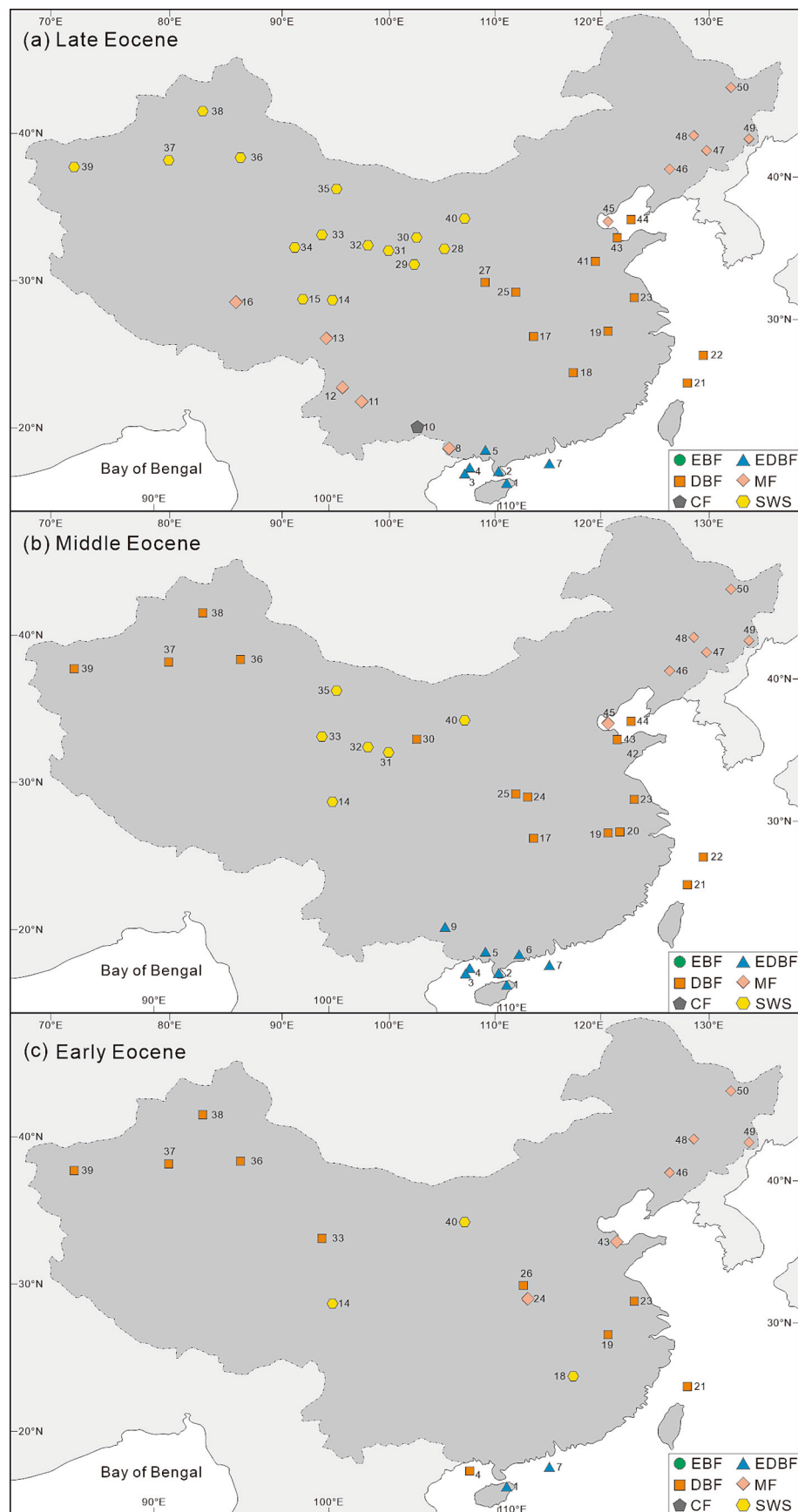


Fig. 10. Reconstruction of Eocene ecosystems in East Asia.

CRediT authorship contribution statement

Jinhua Zeng: Writing – review & editing, Writing – original draft, Software, Project administration, Methodology, Investigation, Formal analysis, Data curation, Conceptualization. **Tao Jiang:** Writing – review & editing, Supervision, Methodology, Funding acquisition, Conceptualization. **Keqiang Wu:** Data curation. **Desheng Hu:** Data curation. **Yong Man:** Data curation. **Licheng Cao:** Supervision, Methodology. **Cong Cheng:** Writing – review & editing, Supervision. **Zigui Chen:** Writing – review & editing, Supervision. **Kun Wang:** Visualization. **Nan Bai:** Data curation. **Meiling Feng:** Formal analysis. **Ziyi Li:** Formal analysis.

Declaration of competing interest

The authors declare that they have no known competing financial interests or personal relationships that could have appeared to influence the work reported in this paper.

Acknowledgements

This research was funded by the National Key Research and Development Program of China [No. 2024YFC2814702], the National Natural Science Foundation of China [No. 42276073 and No. 41976073], the Guangdong Basic and Applied Basic Research Foundation [No. 2023A1515110405 and No. 2025A1515011949].

Appendix A. Supplementary data

Supplementary data to this article can be found online at <https://doi.org/10.1016/j.palaeo.2025.113288>.

Data availability

The authors confirm that all data necessary for supporting the scientific findings of this paper have been provided.

References

- Aleksandrova, G.N., Kodrul, T.M., Jin, J., 2015. Palynological and Paleobotanical Investigations of Paleogene Sections in the Maoming Basin, South China. *Stratigr. Geol. Correl.* 23 (3), 300–325.
- Algeo, T.J., Hong, H., Wang, C., 2025. The chemical index of alteration (CIA) and interpretation of ACNK diagrams. *Chem. Geol.* 671, 122474.
- Anagnostou, E., John, E.H., Edgar, K.M., Foster, G.L., Ridgwell, A., Inglis, G.N., Pancost, R.D., Lunt, D.J., Pearson, P.N., 2016. Changing atmospheric CO₂ concentration was the primary driver of early Cenozoic climate. *Nature* 533, 380–384.
- Beerling, D.J., Royer, D.L., 2011. Convergent Cenozoic CO₂ history. *Nat. Geosci.* 4, 418–420.
- Bosboom, R.E., Dupont-Nivet, G., Houben, A.J.P., Brinkhuis, H., Villa, G., Mandic, O., Stoica, M., Zachariasse, W.J., Guo, Z.J., Li, C.X., Krijgsman, W., 2011. Late Eocene Sea retreat from the Tarim Basin (West China) and concomitant Asian paleoenvironmental change. *Palaeogeogr. Palaeoclimatol. Palaeoecol.* 299, 385–398.
- Bouchenak-Khelladi, Y., Verboom, G.A., Hodkinson, T.R., Salamin, N., Francois, O., Chonghaile, G.N., Savolainen, V., 2009. The origins and diversification of C4 grasses and savanna-adapted ungulates. *Glob. Chang. Biol.* 15, 2397–2417.
- Burke, K.D., Williams, J.W., Chandler, M.A., Haywood, A.M., Lunt, D.J., Otto-Bliesner, B.L., 2018. Pliocene and Eocene provide best analogs for near-future climates. *Proc. Natl. Acad. Sci.* 115 (52), 13288–13293.
- Cai, Y., Kong, X., 2024. Eocene monsoon climate expansion in East Asia: evidence from orbital-cycle driven terrestrial successions in the Jianghan Basin, Central China. *Sedimentology* 71 (5), 1477–1497.
- Cao, H., Jin, S., Sun, M., Wang, H., 2016. Astronomical forcing of sedimentary cycles of late Eocene Liushagang Formation in the Bailian Sag, Fushan Depression, Beibuwan Basin, South China Sea. *J. Cent. South Univ. (Engl. Ed.)* 23, 1427–1428.
- Cao, J., Wu, M., Chen, Y., Hu, K., Bian, L., Wang, L., Zhang, Y., 2012. Trace and rare earth element geochemistry of Jurassic mudstones in the northern Qaidam Basin, northwest China. *Geochemistry* 72 (3), 245–252.
- Chen, L., Deng, W., Su, T., Li, S., Zhou, Z., 2021. Late Eocene sclerophyllous oak from Markam Basin, Tibet, and its biogeographic implications. *Sci. Sin. Terra* 64 (11), 1969–1981.
- Ding, L., Xu, Q., Yue, Y., Wang, H., Cai, F., Li, S., 2014. The Andean-type Gangdese Mountains: Paleoelevation record from the Paleocene–Eocene Linzhou Basin. *Earth Planet. Sci. Lett.* 392, 250–264.
- Ding, L., Spicer, R.A., Yang, J., Xu, Q., Cai, F., Li, S., Lai, Q., Wang, H., Spicer, T.E.V., Yue, Y., Shukla, A., Srivastava, G., Khan, M.A., Bera, S., Mehrotra, R., 2017. Quantifying the rise of the Himalaya orogen and implications for the south Asian monsoon. *Geology* 45 (3), 215–218.
- Fang, X., Yan, M., Zhang, W., Nie, J., Han, W., Wu, F., Song, C., Zhang, T., Zan, J., Yang, Y., 2021. Paleogeography control of Indian monsoon intensification and expansion at 41 Ma. *Sci. Bull.* 66 (22), 2320–2328.
- Farnsworth, A., Lunt, D.J., Robinson, S.A., Valdes, P.J., Roberts, W.H.G., Clift, P.D., Markwick, P., Su, T., Wrobel, N., Bragg, F., Kelland, S.J., Pancost, R.D., 2019. Past East Asian monsoon evolution controlled by paleogeography, not CO₂. *Sci. Adv.* 5, 1697.
- Foster, G.L., Royer, D.L., Lunt, D.J., 2017. Future climate forcing potentially without precedent in the last 420 million years. *Nat. Commun.* 14845, 1–8.
- Greenwood, D.R., Wing, S.L., 1995. Eocene continental climates and latitudinal temperature gradients. *Geology* 23 (11), 1044–1048.
- Guan, J., 2021. Had the Monsoon Climate Existed during the Early Eocene in the SE Tibetan Plateau? - a Case Study from Lacustrine Sediments of the Gonjo Basin. *Yunnan University, Kunming.*
- Guo, B., Nie, J., Li, J., Xiao, W., Pan, F., 2022. Expansion/shrinkage history of the Paratethys Sea during the Eocene: New insights from eolian Red Clay records in the Altyn Mountains, northern China. *Front. Earth Sci.* 10, 1052627.
- Han, Z., 2023. Late Eocene Angiosperm Fossils and Paleoenvironmental Significance in Weinan. *Xi'an shiyou University, Xi'an, Shaanxi.*
- Han, X., Shu, J., 2020. Early Eocene palynological assemblages from Donglutian Coal Mine in Fushun Basin and their paleoclimatic significance. *Global Geology* 39 (1), 72–89.
- He, C., Tao, J., 1997. A study on the Eocene flora in Yilan County. *Heilongjiang. Acta Phytotaxon. Sin.* 35 (3), 249–256.
- Henry, M., Vallis, G.K., 2022. Variations on a pathway to an early Eocene climate. *Paleoceanogr. Paleocl.* 37, 25724525.
- Herman, A.B., Spicer, R.A., Aleksandrova, G.N., Yang, J., Kodrul, T.M., Maslova, N.P., Spicer, T.E.V., Chen, G., Jin, J., 2017. Eocene–early Oligocene climate and vegetation change in southern China: evidence from the Maoming Basin. *Palaeogeogr. Palaeoclimatol. Palaeoecol.* 479, 126–137.
- Hoorn, C., Straathof, J., Abels, H.A., Xu, Y., Utescher, T., Dupont-Nivet, G., 2012. A late Eocene palynological record of climate change and Tibetan Plateau uplift (Xining Basin, China). *Palaeogeogr. Palaeoclimatol. Palaeoecol.* 344–345, 16–38.
- Huang, M., Liu, Y., Chen, F., Tao, Y., Sun, Y., 2024. Correlations of chemical weathering indicators with major chemical constituents in sediments to obtain palaeoclimate information from Chaohu Lake, China. *Sci. Rep.* 14, 17258.
- Huber, M., Caballero, R., 2011. The early Eocene equitable climate problem revisited. *Clim. Past* 7, 603–633.
- Huber, M., Goldner, A., 2012. Eocene monsoons. *J. Asian Earth Sci.* 44, 3–23.
- Kong, X., Jiang, Z., Wu, S., Ge, Y., 2024. Stepwise astronomical tuning of obliquity-driven evaporite cycles in an Eocene salt lake (Jianghan Basin, Hubei Province, China): Implications for middle Eocene East Asian monsoon-like climate evolution. *Geol. Soc. Am. Bull.* 136 (7/8), 3277–3290.
- Lerman, A., 1978. Lakes: Chemistry, Geology, Physics, Springer, New York.
- Li, Z., 1998. Eocene palynology of well LF13-2-1 in Pearl River Mouth Basin. *China Offshore Oil Gas Geol.* 12 (3), 168–173.
- Li, M., 2005. The late cretaceous and Paleogene palynological assemblages from Xuanzhou, Anhui Province. *Acta Micropalaeontol. Sin.* 22 (1), 59–77.
- Li, J., Wang, R., Qin, J., Qiu, K., 2019. Paleogene-Neogene micropaleontological records of the Weixinan Depression, Beibuwan Basin and their paleoenvironmental significance. *Mar. Geol. Quat. Geol.* 40 (2), 29–36.
- Li, Q., Utescher, T., Liu, Y.C., Ferguson, D., Hui, J., Cheng, Q., 2022. Monsoonal climate of East Asia in Eocene times inferred from an analysis of plant functional types. *Palaeogeogr. Palaeoclimatol. Palaeoecol.* 601, 111138.
- Li, G., Shi, J., Fan, T., Hu, D., You, J., Li, Y., Gao, Z., Deng, C., Fan, J., Zhou, G., 2023. Shale lithofacies association types and development models in Eocene lacustrine facies strata constrained by astronomical cycles: a case study of the Liushagang Formation in the Weixinan sag, Beibuwan Basin. *Quat. Sci.* 43 (6), 1614–1629.
- Li, N., Ji, X., Tang, X., Chen, Z., Zhang, T., Xu, Z., Zhu, Y., 2024. Eocene micropaleontology and its environmental significance in the well B1, Xihu Sag, East China Sea Basin. *Acta Micropalaeontol. Sin.* 41 (2), 161–173.
- Licht, A., Cappelle van, M., Abels, H.A., Ladant, J.B., Trabucho-Alexandre, J., France-Lanord, C., Donnadieu, Y., Vandenberghe, J., Rigaudier, T., Lecuyer, C., Terry Jr., D., Adriaens, R., Boura, A., Guo, Z., Soe, A.N., Quade, J., Dupont-Nivet, G., Jaegerl, J.-J., 2014. Asian monsoons in a late Eocene greenhouse world. *Nature* 513 (7519), 501–506.
- Liu, S., 2019. Study on Palaeoenvironment Restoration and Tectonic Evolution of Late Paleogene in Luhe Basin, Nanhua County. *Kunming University of Science and Technology, Kunming, Yunnan Province.*
- Liu, X., Dong, B., Yin, Z., Smith, R.S., Guo, Q., 2017. Continental drift and plateau uplift control origination and evolution of Asian and Australian monsoons. *Sci. Rep.* 7, 40344.
- Liu, Z., Yan, D., Yu, J., Deng, Y., Ding, Y., 2025. Eocene palynoflora and paleoclimate reconstruction in Weixinan sag, Beibuwan Basin. *Acta Pet. Sin.* 46 (2), 355–371.
- Liu, J., Zhang, K., Song, B., Xu, Y., Zhang, J., Huang, W., Zhang, D., 2020. Paleogene–Neogene pollen and climate change in Dahonggou Region of Qaidam Basin. *Geosci* 34 (4), 732–744.

- Luo, W., Xie, J., Liu, X., Hu, W., Zhang, J., Zhou, W., 2013. The study of paleogene climate in the Haizhong Depression, Beibuwan Basin, northern South China Sea. *Acta Micropalaeontol. Sin.* 30 (3), 288–296.
- Ma, Y., Fan, M., Lu, Y., Liu, H., Zhang, S., Liu, X., 2019. Stable isotope record of middle Eocene summer monsoon and its instability in eastern China. *Glob. Planet. Chang.* 175, 103–112.
- Meng, Q., Bruch, A.A., Sun, G., Liu, Z., Hu, F., Sun, P., 2018. Quantitative reconstruction of Middle and late Eocene paleoclimate based on palynological records from the Huadian Basin, northeastern China: evidence for monsoonal influence on oil shale formation. *Palaeogeogr. Palaeoclimatol. Palaeoecol.* 510, 63–77.
- Miao, Y., Fang, X., Song, Z., Wu, F., Han, W., Song, C., 2008. Late Eocene pollen records and palaeoenvironmental changes in northern Tibetan Plateau. *Sci. China Ser. D Earth Sci.* 51, 1089–1098.
- Miao, Y., Wu, F., Chang, H., Fang, X., Deng, T., Sun, J., Jin, C., 2016. A Late-Eocene palynological record from the Hoh Xil Basin, northern Tibetan Plateau, and its implications for stratigraphic age, paleoclimate and paleoelevation. *Gondwana Res.* 31, 241–252.
- Nesbit, H.W., Young, G.M., 1982. Early Proterozoic climates and plate motions inferred from major element chemistry of lutes. *Nature* 299, 715–717.
- Ometimi, E.J., Lenhardt, N., Yang, R., Gotz, A.E., Bumby, A.J., 2022. Sedimentary geochemistry of late Cretaceous-Paleocene deposits at the southwestern margin of the Anambra Basin (Nigeria): Implications for paleoenvironmental reconstructions. *Palaeogeogr. Palaeoclimatol. Palaeoecol.* 600, 111059.
- Pearson, P.N., Palmer, M.R., 2000. Atmospheric carbon dioxide concentrations over the past 60 million years. *Nature* 406, 695–699.
- Pearson, P.N., Dongen van, B.E., Nicholas, C.J., Pancost, R.D., Schouten, S., Singano, J. M., Wade, B.S., 2007. Stable warm tropical climate through the Eocene Epoch. *Geology* 35 (3), 211–214.
- Peng, J., 2021. Paleoclimate Evolution Recorded by the Paleocene-Eocene Sediments and its Driving Mechanism in the Dongying Sag. China University of Petroleum (East China), Qingdao.
- Peng, G., Chen, W., Jia, P., Luo, M., He, Y., Jin, Y., Xu, C., Shan, X., 2023. Middle-late Eocene climate in the Pearl River Mouth Basin: evidence from a Palynological and Geological Element Record in the Xijiang Main Subbasin. *Minerals* 13 (3), 374.
- Quan, C., Liu, Y.C., Utescher, T., 2012a. Paleogene temperature gradient, seasonal variation and climate evolution of Northeast China. *Palaeogeogr. Palaeoclimatol. Palaeoecol.* 313–314, 150–161.
- Quan, C., Liu, Y.C., Utescher, T., 2012b. Eocene monsoon prevalence over China: a paleobotanical perspective. *Palaeogeogr. Palaeoclimatol. Palaeoecol.* 365–366, 302–311.
- Renner, S., 2016. Available data point to a 4-km-high Tibetan Plateau by 40 Ma, but 100 molecular-clock papers have linked supposed recent uplift to young node ages. *J. Biogeogr.* 43, 1479–1487.
- Roy, D.K., Roser, B.P., 2013. Climatic control on the composition of Carboniferous–Permian Gondwana sediments, Khalaspir basin, Bangladesh. *Gondwana Res.* 23 (3), 1163–1171.
- Sayem, A.S.M., Guo, Z., Yang, F., Wu, H., Zhang, C., Xiao, G., He, Z., 2018. Sedimentary and geochemical evidence of Eocene climate change in the Xining Basin, northeastern Tibetan Plateau. *Sci. China Earth Sci.* 61, 1292–1305.
- Scotese, C.R., 2016. PALEOMAP PaleoAtlas for GPlates and the PaleoData Plotter Program. PALEOMAP Project. <http://www.earthbyte.org/paleomap-paleoatlas-for-gplates/>.
- Shi, J., Liu, Z., Liu, R., Du, J., Zhang, J., Liu, F., 2008. Quantitative reconstruction of the Eocene paleoclimate in the Fushun Basin, Liaoning Province. *J. Jilin Univ. (Earth Sci. Ed.)* 38 (1), 5.
- Song, Z., Zhang, D., 1990. Geological age of the Caomuhua gypsum mine in Otog Banner, Nei Mongol with review of research on fossil proteaceous pollen in China. *Acta Palaeontol. Sin.* 29 (3), 257–269.
- Song, Z., Wang, W., Mao, F., 2008. Palynological implications for relationship between aridification and monsoon climate in the Tertiary of NW China. *Acta Palaeontol. Sin.* 47 (3), 265–272.
- Song, S., Tang, Z., Xi, D., Yang, S., 2023. Palynology-based reconstructions for climatic patterns in the Eocene-Oligocene of eastern Asia: Implications of the monsoonal circulation history. *J. Asian Earth Sci.* 257, 105836.
- Spicer, R.A., Herman, A.B., Liao, W., Spicer, T.E.V., Kodrul, T.M., Yang, J., Jin, J., 2014. Cool tropics in the Middle Eocene: evidence from the Changchang Flora, Hainan Island, China. *Palaeogeogr. Palaeoclimatol. Palaeoecol.* 412, 1–16.
- Sun, J., Jiang, M., 2013. Eocene seawater retreat from the Southwest Tarim Basin and implications for early Cenozoic tectonic evolution in the Pamir Plateau. *Tectonophysics* 588 (2), 27–38.
- Sun, X., Wang, P., 2005. How old is the Asian monsoon system? – Palaeobotanical records from China. *Palaeogeogr. Palaeoclimatol. Palaeoecol.* 222, 181–222.
- Sun, X., Wang, D., Zhao, Y., 1985. Paleocene-early Eocene palynological assemblages from the Xiangcheng Group in the Lingbao Basin of Henan. *Bull. Chin. Acad. Geol. Sci.* 11, 127–135.
- Tardif, D., Fluteau, F., Donnadieu, Y., Hir, G.L., Ladant, J.B., Sepulchre, P., Licht, A., Poblete, F., Dupont-Nivet, G., 2020. The origin of Asian monsoons: a modelling perspective. *Clim. Past* 16 (3), 847–865.
- Taylor, S.R., McLennan, S.M., 1985. The Continental Crust: Its Composition and Evolution. Blackwell Scientific Publications, Oxford.
- Tong, C., 1989. The lower Tertiary flour-bearing assemblage in Yunsi, Wenkou and Tailai Sags, Shandong Province. *J. Stratigr.* 13 (3), 219–223.
- Tong, G., Zhen, M., Yuan, H., Liu, J., Li, Y., Wang, W., 2001. A Study of Middle and late Eocene Palynological Assemblages in Jianghan Basin and their Environmental significance. *Acta Geosci. Sin.* 22 (1), 73–78.
- Wang, X., 2003. Palynology, Paleovegetation and Paleoclimate of Middle and Late Paleogene of Northern China. Shandong University of Science and Technology, Qingdao.
- Wang, P., 2005. Global monsoon in a geological perspective. *Chin. Sci. Bull.* 54 (7), 1113–1136.
- Wang, Q., 2022. Eocene Climatic and Chemical Weathering Records in Nangqian Basin, Eastern Tibetan Plateau. Lanzhou University, Lanzhou.
- Wang, K., Yang, J., Li, Z., Li, Z., 1975. On the tertiary sporo-pollen assemblages from Lunpola Basin of Xizang, China and their palaeogeographic significance. *Sci. Geol. Sin.* 4, 366–374.
- Wang, D., Sun, X., Zhao, Y., 1984. The paleocene-Eocene palynoflora from the Tantou Basin in West Henan. *Acta Bot. Sin.* 26 (4), 448–455.
- Wang, D., Sun, X., Zhao, Y., 1986. Palynoflora from late cretaceous to Tertiary in Qinghai and Xinjiang. *Bull. Chin. Acad. Geol. Sci.* 15, 152–165.
- Wang, W., Chen, G.J., Chen, Y.F., Kuang, G.D., 2003. Tertiary palynostratigraphy of the Ningming Basin. *Guangxi. J. Stratigr.* 27 (4), 324–327.
- Wang, D., Lu, S., Han, S., Sun, X., Quan, C., 2013. Eocene prevalence of monsoon-like climate over eastern China reflected by hydrological dynamics. *J. Asian Earth Sci.* 62, 776–787.
- Wang, C., Dai, J., Zhao, X., Li, Y., Graham, S.A., He, D.F., Ran, B., Meng, J., 2014. Outward-growth of the Tibetan Plateau during the Cenozoic: a review. *Tectonophysics* 621, 1–43.
- Wang, J., Peng, J., Cao, Y., Liu, K., Song, M., Liu, H., 2022. Mid-late Eocene Paleoclimate Characteristics and significance in the Dongying Depression: an example from well Hk-1. *Acta Sedimentol. Sin.* 40 (4), 1059–1072.
- Wei, X., 2021. Evolution of the Eocene Sedimentary Environment and Formation Mechanism of Hydrocarbon Source Rocks in the Weixinan Sag. China University of Geosciences, Wuhan.
- Wei, Y., Luo, S., 2005. The discovery of the Eocene sporomorphs in the Sharmu Basin, Sershui, western Sichuan. *Sediment. Geol. Tethyan Geol.* 25 (4), 42–45.
- Wei, X., Lu, J., Liu, L., He, W., Yan, D., Wei, Z., Zou, J., 2018. Astronomical cycle identification and high frequency sequence division of the 1st Member of Liushagang Formation in Weixinan sag, Beibuwan basin. *China Offshore Oil Gas* 30 (6), 99–108.
- Wei, Y., Yang, B., Xia, H., Deng, H., 2021. Paleovegetation and paleoclimate during Mid-late Eocene in Fushun Basin. *Earth Sci.* 46 (5), 1848–1861.
- Wu, J., 2017. Redefinition of Cenozoic Chronostratigraphic Framework and Reconstruction of Paleoenvironment and Paleoelevation in the Jianchang Basin. China University of Geosciences, Wuhan, Southeast of Tibetan Plateau.
- Wu, F., Fang, X., Yang, Y., Dupont-Nivet, G., Nie, J., Fluteau, F., Zhang, T., Han, W., 2022. Reorganization of Asian climate in relation to Tibetan Plateau uplift. *Nat. Rev. Earth Environ.* 3, 684–700.
- Wu, F., Tang, F., Gao, S., Xie, Y., Jiang, Y., Fang, X., Wang, H., 2024. Northward expansion of Cenozoic Asian humid climate recorded by sporopollen. *Palaeogeogr. Palaeoclimatol. Palaeoecol.* 637, 112009.
- Xia, X., Zhang, N., Yu, J., Yi, C., 2015. Eocene-Oligocene palynology and biostratigraphic correlation in the Nanpu Sag, Bohai Bay Basin, N. China. *Acta Micropalaeontol. Sin.* 32 (3), 269–284.
- Xie, J., Li, J., Mai, W., Zhang, H., Cai, K., Liu, X., 2012. Palynofloras and age of the Liushagang and Weizhou formation in the Beibuwan Basin, South China Sea. *Acta Palaeontol. Sin.* 51 (3), 385–394.
- Xie, Y., Wu, F., Fang, X., 2019. Middle Eocene East Asian monsoon prevalence over southern China: evidence from palynological records. *Glob. Planet. Chang.* 175, 13–26.
- Xie, Y., Wu, F., Fang, X., Song, J., Niu, Z., 2022. Late Eocene onset of the East Asian Monsoon in the Qingjiang Basin of Central Jiangxi Province (Southeast China) revealed by a major vegetation transition from desert to forest. *Palaeogeogr. Palaeoclimatol. Palaeoecol.* 602, 111179.
- Yang, R., 1996. Association and time of Eocene sporo-pollen in Hepu Basin. *Guangxi. Guangxi Geology* 9 (3), 32–41.
- Yang, J., 2022. Characteristics of Sporo-Pollen Assemblages and their Paleoenvironment in Coal-Bearing Strata in Pu Yang Basin, Southeastern Yunnan. Kunming University of Science and Technology, Kunming.
- Yang, J., Lu, S., Liu, W., Peng, S., Zhang, Y., 2005. Paleocene climate and stratigraphic era based on the Sporopollen in Lushi Basin. Henan Province. *Geol. Survey Res.* 28 (3), 151–159.
- Yao, Y., 2006. Eocene palynoflora from Changchang Basin, Hainan Island and its bearing on the implications of paleovegetation and paleoclimate. In: Institute of Botany, the Chinese Academy of Sciences, Beijing.
- Yapp, C.J., 2004. Fe(CO₃)OH in goethite from a mid-latitude north American Oxisol: estimate of atmospheric CO₂ concentration in the early Eocene “climatic optimum”. *Geochim. Cosmochim. Acta* 68 (5), 935–947.
- Ye, J., Zhao, N., Yang, B., Xu, J., 2020. Productivity and development model of source rock of the Liushagang Formation in the Weixinan Sag. *Bull. Geol. Sci. Technol.* 39 (1), 105–113.
- Ye, J., Tian, B., Li, D., 2022. Monsoon intensification in East Asia triggered the evolution of its flora. *Front. Plant Sci.* 13, 1046538.
- Yu, J., Zhang, H., Lin, Q., Gu, Y., Zhang, Z., 2003. Geological implications of sporopollenites flora from Tertiary Xining Group in Minhe County, Qinghai Province. *Earth Sci. J. China Univ. Geosci.* 28 (4), 401–406.
- Yuan, Q., Fan, Q., Wei, H., Qin, Z., Li, Q., Du, Y., Wang, M., 2020. The sedimentary environment of the late Eocene Gypsum in Nangqian Basin, Qinghai Province. *J. Salt Lake Res.* 28 (1), 69–77.
- Zachos, J.C., Stott, L.D., Lohmann, K.C., 1994. Evolution of early Cenozoic marine temperatures. *Paleoceanogr. Paleocl.* 9 (2), 353–387.
- Zachos, J., Pagani, M., Sloan, L., Thomas, E., Billups, K., 2001. Trends, Rhythms, and Aberrations in Global climate 65 Ma to present. *Science* 292, 686–693.

- Zachos, J.C., Dickens, G.R., Zeebe, R.E., 2008. An early Cenozoic perspective on greenhouse warming and carbon-cycle dynamics. *Nature* 451, 279–283.
- Zeng, J., Lan, X., Liu, H., Wei, Y., 2022. Genesis and mechanisms of organic matter enrichment of the Hongshizhuang Formation in the Zhoukoudian area of Jingxi sag, North China. *J. Palaeogeogr.* 11 (4), 1–25.
- Zhang, Y., 1981. Tertiary spores and pollen grains from the Leizhou Peninsula. *Acta Palaeontol. Sin.* 20 (5), 449–458.
- Zhang, S., 2015. Reconstruction of palaeovegetation and palaeoenvironment community of Pinghu Formation in Xihu Sag by geochemical method. China University of Geosciences (Beijing), Beijing.
- Zhang, Y., Qian, Z., 1992. Eocene palynofloras from the Dainan and Sanduo Formations in north Jiangsu with special reference to Eocene climatic changes in Southeast China. *Acta Micropalaeontol. Sin.* 9 (1), 1–24.
- Zhang, Y., Wang, K., Wang, Y., Wang, J., Wang, R., Wang, C., Qian, S., 1986. Paleogene sporo-pollen assemblages of Nanling Basin in Anhui province and their geological significance. *Oil Gas Geol.* 7 (1), 75–81.
- Zhang, Y., Wang, K., Liu, J., Zheng, Y., 1990. Eocene palynoflora from the Southwestern Continental Shelf Basin of the East China Sea. *Acta Micropalaeontol. Sin.* 7 (4), 389–402.
- Zhang, S., Liu, Y., Li, M., 2010. Eocene-Miocene palynological assemblages in Wanchang area of Jilin and their stratigraphic significance. *Global Geol.* 29 (3), 357–362.
- Zhang, Z., Flatøy, F., Wang, H., Bethke, I., Bentsen, M., Guo, Z., 2012. Early Eocene Asian climate dominated by desert and steppe with limited monsoons. *J. Asian Earth Sci.* 44, 24–35.
- Zhang, T., Yin, F., 2005. Sporopollen assemblage from the Shahejie Formation in the Tanhai area of Huanghua depression. *J. Northwest Univ., Nat. Sci. Ed.* 35 (1), 91–95.
- Zhang, Z., Zhang, Z., He, Z., Tan, N., Guo, Z., Zhu, J., Steinig, S., Donnadieu, Y., Ladant, J.-B., Chan, W.-L., Abe-Ouchi, A., Niezgodzki, I., Knorr, G., Hutchinson, D.K., Boer de, A.M., 2022. Impact of Mountains in Southern China on the Eocene Climates of East Asia. *J. Geophys. Res. Atmos.* 127 (17) e2022JD036510.
- Zhao, Y., Sun, X., Wang, D., 1982. Tertiary Sporopollen assemblages from Shache and Kuche Basin. Xinjiang. *Bull. Chin. Acad. Geol. Sci.* 4, 95–125.
- Zhao, X., Zhang, C., Wu, H., Ren, X., Chang, L., Guo, Z., 2015. Significance of Eocene-Oligocene transition pollen record from Xining Basin, China. *Quat. Sci.* 35 (6), 1489–1498.
- Zhao, Y., Wang, H., Yan, D., Jiang, P., Chen, S., Zhou, J., Ma, J., Qin, C., He, J., Zhao, Y., 2020. Sedimentary characteristics and model of gravity flows in the eocene Liushagang Formation in Weixinan depression, South China Sea. *J. Pet. Sci. Eng.* 190, 107082.
- Zhu, J., Poulsen, C.J., Tierney, J.E., 2019. Simulation of Eocene extreme warmth and high climate sensitivity through cloud feedbacks. *Sci. Adv.* 5 (9), 1874.
- Zoura, D., Haywood, A.M., Hill, D.J., Dolan, A.M., Tang, Z., 2020. The role of Central Asian uplift in East Asian Monsoon circulation and its palaeoclimate implication. *Glob. Planet. Chang.* 184, 103073.